Enhanced Cd phytoextraction by rapeseed under future climate as a consequence of higher sensitivity of HMA genes and better photosynthetic performance

Reference:
Diksaityte Austra, Kniuipyt Inesa, Abdel-Maksoud Mostafa A., Asard Han, Abd Elgawad Hamada.- Enhanced Cd phytoextraction by rapeseed under future climate as a consequence of higher sensitivity of HMA genes and better photosynthetic performance
The science of the total environment - ISSN 1879-1026 - 908(2024), 168164
Full text (Publisher's DOI): https://doi.org/10.1016/J.SCITOTENV.2023.168164
To cite this reference: https://hdl.handle.net/10067/2020770151162165141

Enhanced Cd phytoextraction by rapeseed under future climate as a consequence of higher sensitivity of HMA genes and better photosynthetic performance

Austra Dikšaitytė[a,*], Inesa Kniuipytė[b], Jūratė Žaltauskaitė[a], Mostafa A. Abdel-Maksoud[c], Han Asard[d], Hamada AbdElgawad[d]

[a]Department of Environmental Sciences, Vytautas Magnus University, Universiteto st. 10, LT-53361 Akademija, Kaunas distr., Lithuania

[b]Lithuanian Energy Institute, Laboratory of Heat–Equipment Research and Testing, Breslaujos st. 3, LT-44403, Kaunas, Lithuania

[c]Department of Botany and Microbiology, College of Science, King Saud University, Riyadh 11451, Saudi Arabia

[d]Integrated Molecular Plant Physiology Research, Department of Biology, University of Antwerp, Antwerp, Belgium

[*]Corresponding author at: Department of Environmental Sciences, Vytautas Magnus University, Universiteto st. 10, LT-53361 Akademija, Kaunas distr., Lithuania

E-mail address: austra.diksaityte@vdu.lt (A. Dikšaitytė)

ABSTRACT

This study aimed to investigate the underlying physiological, biochemical, and molecular mechanisms responsible for *Brassica napu's* potential to remediate Cd-contaminated soil under current (CC) *vs.* future (FC) climate (400 *vs.* 800 ppm of CO_2, 21/14 °C *vs.* 25/18 °C). *B. napus* exhibited good tolerance to low Cd treatments (Cd-1, Cd-10, i.e., 1, 10 mg kg^{-1}) under both climates without visible phytotoxicity symptoms. TI sharply decreased by 47% and 68% ($p < 0.05$), respectively, in Cd-50 and Cd-100 treated shoots under CC, but to a lesser extent (−26% and −53%, $p < 0.05$) under FC. This agreed with increased photosynthetic apparatus performance under FC, primarily due to a significant decrease in the closure of active PSII RCs ((dV/dt)o, TRo/RC) and less dissipated excitation energy (DIo/RC, φDo). Calvin Benson cycle-related enzyme activity also improved under FC with 2.2-fold and 2.4-fold ($p < 0.05$) increases in Rubisco and TPI under Cd-50 and Cd-100, respectively. Consequentially, a 2.2-fold and 2.3-fold ($p <$

0.05) boosted P_r resulted in a 2.3-fold and 2.4-fold ($p < 0.05$) increase in the DW of Cd-50 and Cd-100 treated shoots, respectively. This also led to a decrease (26%, $p < 0.05$) in shoot Cd concentration under both high Cd treatments with a slight reduction in BCF. Translocation factor (TF) decreased (on average 42%, $p < 0.05$) by high Cd treatments under both climates. However, under Cd-100, FC increased TF by 1.7-fold ($p < 0.05$) compared to CC, which could be explained by significant increases in the expression of HMA genes, especially *BnaHMA4a* and *BnaHMA4c*. Finally, Cd TU increased under FC by 65% and 76% ($p < 0.05$) under Cd-50 and Cd-100. This led to a shorter hypothetical remediation time for reaching the Cd pollution limit by 35 ($p > 0.05$) and 61 ($p < 0.05$) years, respectively, compared to CC.

Keywords: *Brassica napus*, Future climate, HMA genes, Photosynthetic apparatus performance, CBC-related enzymes, Phytoextraction potential.

1. Introduction

Increased anthropogenic activities including mining, smelting, disposal of manure, wastewater, or sewage sludge and indiscriminate use of phosphate fertilizers and pesticides have resulted in widespread soil contamination with heavy metals (HMs) (Dutta et al., 2021; Haider et al., 2021; Yan et al., 2020). Among these HMs, cadmium (Cd) is a non-essential element known for its harmful effect on plant growth and physiology (Dutta et al., 2021; Sabir et al., 2020). Cd is highly phytotoxic even at low concentrations (Ali et al., 2017; Gallego et al., 2012; Jiang et al., 2016; Yang et al., 2017). For example, most plants exhibit visible Cd toxicity symptoms when the bioavailable Cd concentration exceeds 0.001 mg kg^{-1} or reaches 3-30 mg kg^{-1} in plant tissues (Dutta et al., 2021). Cd accumulation in plant induces many morphological, physiological, and biochemical toxic effects on plant growth and development, with the photosynthetic apparatus, especially the photosystems I (PSI) and II (PSII), being the primary site of Cd action (Haider et al., 2021; He et al., 2017). Depending on continent and country, Cd concentrations in unpolluted soils range from 0.01 to 1 mg kg^{-1} with a global mean of 0.36 mg kg^{-1} and a European average of 0.2 mg kg^{-1} (Dutta et al., 2021; Kubier et al., 2019). Soil Cd content of more than 3 mg kg^{-1} is considered a critical Cd pollution limit (Dutta et al., 2021). However, soil Cd levels near industrial and agricultural activities far exceed this limit, reaching > 150 mg kg^{-1} (Ali et al., 2017). Unlike organic contaminants, Cd is non-biodegradable and therefore persists for a long time after being introduced into the soil (Suman et al., 2018; Yan et al., 2020). Moreover, Cd is one of the most mobile elements in the environment (Kubier et al., 2019), with the highest solubility in water (Hussain and Keçili, 2020) and thus can be quickly taken up by plants (Hussain et al., 2021). This, however, facilitates Cd removal from the soil via phytoextraction, which is a safe, clean, cost-effective plant-based technology to translocate the soil's heavy metals to aboveground harvestable biomass of plants (Khalid et al., 2017; Diarra et al., 2021). In recent years, phytoextraction has become the most prominent phytoremediation method for extracting HMs from polluted soil (Yan et al., 2020).

One important criterion that must be considered during plant selection for phytoextraction is climatic and soil conditions (Suman et al., 2018). Change in climatic conditions influences the plant-heavy metal interaction (Rajkumar et al., 2013). Therefore, it is important to investigate the future climate (FC) effect on phytoextraction performance. Atmospheric CO_2 concentration continues to rise, reaching annual averages of 415 ppm in 2022 (Lindsey, 2022). It is expected to roughly double from current levels by 2100 (IPCC, 2021) under the SSP3-7.0 scenario with high greenhouse gas (GHG) and CO_2 emissions (IPCC, 2021). The global surface temperature will also continue to increase until at least mid-century, adding 2.8 to 4.6 °C by the end of this century (2081-2100), compared to 1850-1900, under the high GHG emissions scenario (IPCC, 2021). However, Europe has been experiencing a warming trend that is more rapid than the global average from 1991 to 2021, which was more than twice as fast as the global average, about +0.5 °C per decade (WMO, 2022). According to the Coupled Model Intercomparison

Project phase 6 (CMIP6) and SSP3-7.0 scenarios, Europe's projected land temperature rise by the end of the century will be +4.26 °C on average, relative to the historical baseline of 1995-2014 (Tebaldi et al., 2021).

The effects of elevated CO_2 concentration (eCO_2) and warming on plant growth and metal accumulation have been shown to significantly differ depending on the environment's physical-chemical-biological features and the plant species (Rajkumar et al., 2013). eCO_2 has a positive effect on Cd phytoremediation in polluted soils, owing to the significant increase in plant biomass (Jia et al., 2010; Li et al., 2010), metal accumulation (Guo et al., 2015, 2011) or both (Li et al., 2010). On the other hand, decreases in Cd concentrations in different plant organs have also been reported under eCO_2 (Jia et al., 2010; Li et al., 2010) or higher air temperature conditions (Li et al., 2012; Ma et al., 2017; Rabêlo et al., 2020). Predicted elevated temperatures are expected to increase the pollutant's toxicity but will accelerate chemical degradation also (Noyes et al., 2009). Therefore, the overall change in phytoextraction efficiency remains unclear and depends on the climatic variable's effects on plant metabolism, and the phytoextraction could increase or decrease.

Another vital point for effective phytoextraction is the appropriate selection of an efficient plant capable of growing in a contaminated environment and transferring toxic contaminants to its aboveground organs (Khalid et al., 2017; Suman et al., 2018; Yan et al., 2020). Among the characteristics that determine the phytoextraction potential of a plant species, the key factors are metal-accumulating capacities and aboveground biomass (Yan et al., 2020). In this regard, *B. napus*, a fast-growing crop, is known for high-stress tolerance and the ability to sequester Cd in Cd-contaminated soils, promoting long-term soil decontamination (Li et al., 2018; Rizwan et al., 2018; Suman et al., 2018). Furthermore, oilseed crops have the advantage over other Cd-tolerant plants because they can generate by-products, such as biofuels, which contribute to the economy (Rizwan et al., 2018; Romih et al., 2012; Sebastian and Prasad, 2014). Regarding metal-accumulating capacities, some members of the heavy metal P_{1B}-ATPase (HMA) family, which function as transporters to hydrolyze ATP for the transport of metal ions (Argüello et al., 2007), are responsible for Cd translocation in various plant species and play a vital role in Cd detoxification (Li et al., 2018). For example, in rice, *OsHMA2* is linked to vascular tissue zinc loading and tonoplast localization (Yamaji et al., 2013). In *Arabidopsis thaliana* and rice, *HMA3* is predominantly expressed in roots, limiting Cd translocation to shoots by selectively sequestrating Cd into root vacuoles (Chao et al., 2012; Ueno et al., 2010). Meanwhile, *OsHMA4* functions to sequester Cu into root vacuoles, limiting Cu accumulation in the grain (Huang et al., 2016). *HvHMA1* plays a role in Zn and Cd transport into barley grain (Mikkelsen et al., 2012). HMA genes also play a significant role in Cd translocation in wheat, in which they are localized in the plasma membrane (Tan et al., 2013). In *A. thaliana*, overexpression of *AtHMA3* resulted in a 2- to 3-fold increase in Cd accumulation compared to wild-type plants (Morel et al., 2009). There is also evidence of several HMA genes, e.g., *BnHMA2;2*, *BnHMA2;3*, *BnHMA2;5* (Li et al., 2018) and *BnaHMA4c* (Zhang et al., 2020), responding to Cd stress in *B. napus*.

Recently, *B. napus* demonstrated high Cd tolerance and ability to Cd phytoextraction from low and moderate Cd-polluted soil but showed low Cd removal efficiency in highly Cd-contaminated soil under current climate (CC) conditions (Kniuipytė et al., 2023). Meanwhile, our previous studies have shown that eCO_2 and higher air temperature conditions improved *B. napus* biomass production and photosynthetic performance (Dikšaitytė et al., 2020, 2019; Juozapaitienė et al., 2019). Therefore, we hypothesized that FC conditions with eCO_2 and increased temperature could enhance Cd phytoextraction potential of *B. napus*. This study aimed to investigate the physiological, biochemical, and molecular mechanisms that link metal-accumulating capacities and photosynthetic performance with phytoextraction efficiency in *B. napus*. To this end, we deeply investigated the expression of HMA genes, underlying Cd transfer efficiency from roots to shoots, photosynthetic apparatus performance, and

Calvin-Benson cycle (CBC)-related enzyme activity in response to Cd-induced stress under CC and FC conditions.

2. Materials and methods

2.1. Experimental materials and soil preparation

The rapeseed (*Brassica napus* L., var. 'Fenja') seeds were obtained from the Institute of Agriculture of the Lithuanian Research Centre for Agriculture and Forestry. The pot experiment was conducted in controlled environment growth chambers (10 m^3 chamber volume, 2.0 × 2.0 × 2.5 m width, length, height). The used field soil (*Calcari-Endohypogleyic Luvisol*) of the top layer (0-20 cm deep) was collected from the Academy of Agriculture Experimental Research Station of Vytautas Magnus university (Kaunas district, Lithuania). The soil was grounded into particles up to 10 × 10 mm in size and mixed with agroperlite and sand (fraction 0-2 mm) in a 5:3:2 volume ratio. The prepared soil was placed in 3-liter vegetation pots (2.5 kg) and 60 kg N ha^{-1} of complex NPK commercial fertilizer (12-11-18 + microelements) (Achema, Lithuania) was applied. Before soil fertilization, the main physical and chemical characteristics of the prepared soil, such as pH (ISO 10390), mineral nitrogen ($N_{min,}$ N-NO_3 + N-NO_2 and N-NH_4, ISO 13395 and ISO 11732), plant-available P and K determined by Egner-Riehm-Domingo (A-L) method (Egnér et al., 1960), plant-available S, Ca, and Mg (LVP D-12:2021 and LVP D-13:2021 standards), soil organic carbon (C, ISO 10694), humus (ISO 10694), soil organic matter (SOM, ISO 10694), and electrical conductivity (EC, ISO 11265) were analyzed (Table S1). Before the experimental analyses, soil samples were air-dried and sieved through a 2-mm mesh.

2.2. Experimental design and growth conditions

The experiment was carried out in a completely randomized block design using two factors (Cd and climate). Five Cd concentrations (0, 1, 10, 50, and 100 mg kg^{-1}) and two climate conditions (current climate (CC) and future climate (FC)) were applied. Three replicates for each Cd treatment (supplied as $CdCl_2 \times 2.5H_2O$), designated as Cd-0, Cd-1, Cd-10, Cd-50, and Cd-100, were prepared for CC and FC, yielding a total of 30 experimental units. Half of the pots contained different Cd concentrations were placed in growth chamber with CC conditions (the air temperature (Tair) of 21/14 °C (day/night), corresponding to the long-term average temperature of the vegetation period in Lithuania, 400 ppm atmospheric CO_2 concentration and relative air humidity (RH) of 55-60/65-70% (day/night)). The second half of the pots placed in growth chamber with FC conditions (Tair of 25/18 °C, 800 ppm of CO_2, and RH of 45-50/55-60%). Other growing conditions in both chambers were maintained identically: a 14 h photoperiod per day and ~ 300 mol m^{-2} s^{-1} photosynthetically active radiation (PAR) at the top of the plant height. PAR was provided by a combination of natural daylight luminescent lamps (Philips, Waterproof OPK Natural Daylight LF80 Wattage 2 × 58 W/TL-D 58 W) and high-pressure sodium lamp (Philips MASTER GreenPower CG T 600 W). The CO_2 concentration was automatically controlled by adjusting the amount of injected CO_2 gas and the chamber conditioner. Tair in the growth chambers was manually controlled at the operating cupboards (Emerson Network Power S.r.l., Italy, model No. S06UC021V300020FX051260) of the growth chambers. The IGSS 9–13175 software was used to control the climate program. Tair, RH, and CO_2 were measured using an automated sensor (CO2HRT-D, Regin, Källered, Sweden) placed in both chambers.

The prepared soil with embedded Cd was left for stabilization in the chambers for seven days under CC and FC conditions. Then fifteen rapeseed seeds were sown in a pot. On the 21st day after sowing (DAS), plants were thinned, leaving seven units per pot. On the 34th DAS, all plants were fertilized again with the complex NPK fertilizer (NPK 12-11-18 + microelements) at a rate of 60 kg N ha^{-1}. Throughout the experiment, plants grown in both chambers were regularly watered with tap water to maintain a volumetric soil water content (SWC) of 30%, as measured with a Theta Probe ML2x sensor in conjunction with a handset HH2 moisture meter at a depth of 6 cm (Delta-T Devices Ltd., Cambridge, UK). To avoid an "edge" effect on plant growth, pots in the same chamber were rotated every other day. Moreover, to prevent a possible chamber effect on plant growth, all plants were transferred from one chamber to another twice during the experiment, re-establishing the required climatic conditions. The morphological parameters for treatment comparisons were assessed on the 64th DAS, while physiological parameters were measured one day earlier (63 DAS).

2.3. Analysis of gene expression

To investigate the molecular mechanism of Cd tolerance in *B. napus*, the expression levels of homologous HMA1-4 genes under CC and FC conditions were evaluated using a quantitative real-time polymerase chain reaction (qRT-PCR). The TransZol kit was used to extract total RNA from rapeseed radicles grown under control (Cd-0) or Cd stress (Cd-1, Cd-10, Cd-50, and Cd-100) conditions (Trans Gene Biotech) (Huang et al., 2012). The first strand cDNA was synthesized with 500 ng RNA using the HiScript® II Q Select RT SuperMix for qPCR (+gDNA wiper) kit (Vazyme Biotech) according to the manufacture protocol. The gene copy-specific primers for homologous genes were created using Primer Premier 5 (Table S2). The qRT-PCR assay was performed in the LightCycler® 480 qPCR machine (Roche Life Science) using the LightCycler® 480 SYBR Green I Master kit following the manufacturer's instructions. BnACTIN7's relative expression levels were normalized using the △CT method (Zhang et al., 2018).

2.4. Evaluation of photosynthetic apparatus performance

A plant efficiency analyzer (Handy PEA, Hansatech Instruments, King's Lynn, Norfolk, England) was used to measure chlorophyll *a* fluorescence (ChlF). The youngest fully expanded leaves were dark-adapted for 15 min before being illuminated with a saturating ultra-bright red-light pulse (650 nm, 1800 mol photons m^{-2} s^{-1}) from an array of three light-emitting diodes, which provided uniform illumination over the area of leaf exposed by the leaf clip (4 mm dia). The light pulse generates a fast fluorescence rise from the initial fluorescence intensity (F_0) when all reaction centers are open to a maximal (F_m) when all reaction centers are closed. The data from 1-sec measurements were used to calculate various biophysical parameters derived from the OJIP transients using the JIP-test equations (Strasser et al., 2010, 2004, 2000). JIP-test is a mathematical model developed as a biophysical tool for assessing the cascade of chloroplast redox reactions at microsecond or millisecond scales (Kalaji et al., 2016) based on the theory of 'energy flow' across thylakoid membranes (Strasser et al., 2000). The JIP-test parameters, their abbreviations, formulas, and definitions used in this study are presented in Table S3.

2.5. Determination of photosynthetic and antioxidant pigment content

High-performance liquid chromatography (HPLC) (silica-based C18 column; Waters Spherisorb 5 m ODS1 4.6 250 mm) was used to determine the content of photosynthetic and antioxidant pigments after separation on a reverse phase, as described by de Sousa et al. (2022). Acetonitrile (C_2H_3N), methanol (CH_3OH), and water (H_2O) in the ratio 81:9:10 were used as solvent A, and methanol (CH_3OH) and ethyl acetate ($C_4H_8O_2$) (68:32) was used as solvent B. A diode array detector (LC-10ADvp, Shimadzu, Tokyo, Japan) was used to detect molecules.

2.6. CBC-related enzyme's activity measurements

The activity of ribulose 1,5-bisphosphate carboxylase/oxygenase (RuBisCO) enzyme was measured in leaf extracts using a modified Wang and Portis (1992) method as it was previously described by de Sousa et al. (2022). RuBisCO activity was measured after NADH oxidation (340 nm) (Racker, 1962), and relative Rubisco levels were measured as described earlier by Soares et al. (2016). Activities of fructose 1,6-bisphosphatase (FBPase) (EC 3.1.3.11), triose-phosphate isomerase (TPI) (EC 1.2.1.12), phosphoglycerate kinase (PGK) (EC 2.7.2.3), glyceraldehyde 3-phosphate dehydrogenase (GAPDH) (EC 1.2.1.12), and aldolase (ALS) (EC 4.1.2.13) were also measured following NADH oxidation at 340 nm. TPI activity was measured according to Aoyagi and Bassham's (1983) method, PGK and GAPDH based on Latzko and Gibbs's (1968) description, and ALS using the Russell and Gibbs (1967) procedure. All these photosynthetic enzyme assays have been described previously by de Sousa et al. (2022).

2.7. Evaluation of gas exchange

The photosynthetic rate (P_r, µmol CO_2 m^{-2} s^{-1}), stomatal conductance (g_s; mol H_2O m^{-2} s^{-1}), transpiration rate (E; mmol H_2O m^{-2} s^{-1}), the ratio of intercellular to ambient CO_2 concentration (C_i/C_a), and water use efficiency (WUE, µmol CO_2 $mmol^{-1}$ H_2O, determined by P_r / E) were estimated using a portable LI-6400 infrared gas-exchange system (Li-6400, LI-COR Inc., NE, USA), calibrated according to the specifications of manufacturer. The youngest fully expanded leaves of three randomly chosen plants per pot with three pots per treatment were measured. Measurements were taken after CO_2 and H_2O flux stabilization to ensure that photosynthetic responses reflected those within the growth chambers (Dan Wang et al., 2014). CO_2 concentration and temperature in the leaf cuvette were maintained under plants' growth conditions. In CC, leaf chamber conditions were controlled at 21 °C (block temperature) and 400 µmol mol^{-1} CO_2 concentration of the reference cell, resulting in a mean leaf cuvette CO_2 concentration of 397 ± 0.4 µmol mol^{-1}. In FC, block temperature and CO_2 concentration of the reference cell were set at 25 °C and 800 µmol mol^{-1}, resulting in a mean leaf cuvette CO_2 concentration of 794 ± 0.5 µmol mol^{-1}. After achieving a steady state under those conditions (usually in 5-10 min), measurements were automatically logged for 5 min every 15 sec. The air flow rate through the assimilation chamber was maintained at 500 µmol s^{-1}. The humidity (RH) inside the leaf cuvette were allowed to vary depending on the conditions in the plant's growth chambers. PAR outside the leaf chamber under CC and FC was 214 ± 0.7 and 219 ± 2.3 μmol m^{-2} s^{-1} on average ($p > 0.05$), respectively.

2.8. Determination of biomass and Cd concentration

Then separated shoots and roots biomass of all seven rapeseeds in the pot was determined based on constant dry weights (DW) (g) after drying in a forced-air ventilation oven at 70 °C. After oven-drying, milled (Retsch MM400, Germany) samples (~ 0.2 g) were microwave-digested (Milestone ETHOS One, Italy) with 65% HNO_3 and 30% H_2O_2 solutions (v/v = 8/2) and Cd concentration was determined by inductively coupled plasma optical emission spectrometry (ICP-OES) on an Optima 8000 (PerkinElmer, USA) (Wheal et al., 2011). The accuracy of the analytical methods was verified using certified reference material CRM − BCR − 129 Hay Powder (Institute for Reference Materials and Measurements) and blank reagent samples. The Cd standard was analyzed every 20 samples to monitor the ICP-OES signal drift, with each sample being scanned three times.

2.9. Evaluation of phytoextraction efficiency

Cd phytoextraction efficiency by rapeseed under CC and FC was estimated by calculating the bioconcentration factor (BCF) and translocation factor (TF) (Ali et al., 2013), Cd-tolerance index (TI) for shoots (Antoniadis et al., 2017) and the shoot total cadmium uptake (TU) index (Dos Santos Utmazian et al., 2007) according to eq. 1–4.

$$\text{BCF} = \frac{C_{shoot}}{C_{soil}} \tag{1}$$

where C_{shoot} is Cd concentration (mg kg^{-1} DW) in shoot and C_{soil} is Cd concentration (mg kg^{-1}) in soil.

$$\text{TF} = \frac{C_{shoot}}{C_{root}} \quad (2)$$

where C_{root} is Cd concentration (mg kg^{-1} DW) in root.

$$\text{TI} = \frac{\textit{Shoot DW in Cd polluted soil}}{\textit{Shoot DW in non-polluted soil}} \quad (3)$$

$$\text{TU} = C_{shoot} \times \textit{Shoot DW} \quad (4)$$

In addition, based on Cd TU for shoots per pot in a unit of area per time, Cd phytoextraction potential for Cd-1–Cd-100 treatments under CC and FC conditions was calculated (eq. 5). The hypothetical remediation time (HRT) required to reduce Cd-contaminated soil to Cd pollution limit of 3 mg kg^{-1} (Dutta et al., 2021) or lower soil guideline value (SGV) based on ecological risk of 10 mg kg^{-1} (Tóth et al., 2016) was calculated according to eq. 6 (adapted from Antoniadis et al., 2017 and Rabêlo et al., 2020).

$$\text{Phytoextraction potential (kg ha}^{-1}\text{ year}^{-1}\text{)} = \frac{\text{TU} \times n_{\textit{number of plants in pot}}}{area/time} \quad (5)$$

where *area* is the area of the pot used in this study (0.0266 m^2) and *time* is the time (in days = 43 days) of plant growth from the thinning to seven units in a pot (n = 7).

$$\text{Hypothetical remediation time (years)} = \frac{Cd_{soil} - Cd_{\textit{pollution limit or SGV}}}{\textit{Phytoextraction potential/SWH}} \quad (6)$$

where Cd_{soil} is the Cd concentrations (mg kg^{-1}) in soil, *SGV* is the soil guideline value (the lower SGV of 10 mg kg^{-1} based on ecological risk, according to Tóth et al. (2016) was used in this study), and *SWH* (kg ha^{-1}) is the weight of soil (in kg) on one hectare, calculated by multiplying the area of a hectare (10 000 m^2) by a depth of the arable layer (assumed to be 0.15 m) and by the bulk density of the soil used in this study (1200 kg m^3).

2.10. Statistical analysis

All statistical analyses were performed using the STATISTICA 8 software after ensuring the data normality and homoskedastic. To compare the means of the measured variables between climates within each Cd concentration and the measured variables between Cd concentrations within each climate, one-way analysis of variance (ANOVA) was used, followed by post hoc all pairwise multiple comparison tests (Fishers' LSD). The two-way ANOVA was used to assess the effects of Cd, climate, and their interaction on the tested parameters. Pearson's correlation analysis was applied to evaluate the relationship between the variables under consideration. The graphs were created using excel software, and the results were expressed as means ± standard error (SE). In all statistical analyses, were fixed effects, and a p-value ≤ 0.05 was the threshold for significance. Hierarchical Clustering Heatmaps were plotted by the SRpolt tool (https://www.bioinformatics.com.cn/en) using the Euclidean distance and the complete linkage method.

3. Results

3.1. Expression of HMA genes involved in HM translocation

In the presence of Cd, *B. napus* showed up-regulation of four HMA family genes under CC conditions and eight under FC. The expressions of *BnaHMA1a*, *BnaHMA1b*, *BnaHMA2a*, and *BnaHMA4c* were increased under both climates, and *BnaHMA2b*, *BnaHMA3a*, *BnaHMA3b*, and

BnaHMA4a only under FC (Fig. 1A-H). Under CC conditions, the expression level of *BnaHMA1a* and *BnaHMA4c* genes was significantly increased in Cd-10–Cd-100 treatments (Fig. 1A, H), and *BnaHMA1b* and *BnaHMA2a* in high (Cd-50 and Cd-100) treatments only (Fig. 1B, C). Under FC, *BnaHMA4c* expression was 1.8 to 4.9 times ($p < 0.05$) up-regulated in both low and high Cd treatments compared to their respective control. However, the expression level of all other HMA1-4 genes was significantly increased only in high Cd treatments. *BnaHMA1a*, *BnaHMA1b*, *BnaHMA2a*, and *BnaHMA2b* expression was significantly up-regulated in Cd-50 and Cd-100 treatments (Fig. 1A-D), while *BnaHMA3a*, *BnaHMA3b*, and *BnaHMA4a* only in Cd-100 (Fig. 1E-G). All *BnaHMA* genes were influenced by Cd, meanwhile the climate and Cd × climate interaction had no significant effect on *BnaHMA1a*, *BnaHMA1b*, and *BnaHMA3a* genes (Table S4). Under both climates, the most up-regulated was the expression of *BnaHMA2a* and *BnaHMA4c* genes. The expression level of *BnaHMA2a* increased by 2.4 and 3.3 times ($p < 0.05$) in Cd-50 and by 2.7 and 4.6 times ($p < 0.05$) in Cd-100 under CC and FC conditions, respectively. *BnaHMA4c* expression was up-regulated by 2.1 and 3.1 times ($p < 0.05$) in Cd-50 and by 2.2 and 4.9 times ($p < 0.05$) in Cd-100 under CC and FC conditions (Fig. 1C, H).

3.2. Photosynthetic apparatus performance

The deleterious Cd effect on photosynthetic apparatus performance was more pronounced under CC than FC conditions (Fig. 2A and B). Twenty-nine of the thirty-three JIP-test parameters analyzed were significantly ($p < 0.05$) affected by Cd treatment under CC conditions (Table S5). The values of Fm, Fv, Fv/Fo, tFm, Area, Sm, φPo, ψEo, φEo, δRo, φRo, REo/RC, RC/ABS, ABS/CSm, TRo/CSm, ETo/CSm, REo/CSm, RC/CSm, PIabs, PItotal, SFIabs, DFabs, and DFtotal parameters were significantly decreased, while dVG/dto, (dV/dt)o, φDo, ABS/RC, TRo/RC, and DIo/RC showed increases compared to control. Only high Cd treatments significantly affected these JIP-test parameters (Fig. S1C) with Fm, Fv, Fv/Fo, φPo, φEo, φDo, ABS/RC, TRo/RC, DIo/RC, REo/RC, ABS/CSm, TRo/CSm, ETo/CSm, and DFabs changing from control plants only in Cd-100 (Fig. 2A and Table S5). The only exception is PItotal, which showed a significantly higher value in Cd-10 ($p < 0.05$). Under FC conditions, significant differences from the respective control (Cd-0 under FC) were observed in sixteen JIP-test parameters, with tFm, Area, Sm, φRo, RC/ABS, REo/CSm, RC/CSm, PIabs, PItotal, SFIabs, and DFtotal decreasing, while dVG/dto, (dV/dt)o, ABS/RC, TRo/RC, and ETo/RC increasing (Figs. 2B and S1C, Table S5). Of these, dVG/dto and (dV/dt)o were significantly affected by Cd-10–Cd-100 treatments, tFm – by Cd-50 and Cd-100, and all others only by Cd-100.

As for the extracted and technical ChlF parameters, the most noticeable variations were observed in dVG/dto and (dV/dt)o, which increased up to 3.2 and 2.7 times by Cd-100 treatment under CC and by 76% and 67% under FC conditions, respectively (all $p < 0.05$) (Fig. 2A, B and Table S5). Among the yield and efficiency parameters, the most obvious negative Cd influence was observed in φRo, which was reduced by 57% and 17% ($p < 0.05$) under CC and FC conditions. In the specific energy fluxes per active PSII RC, the most notable changes occurred in ABS/RC, TRo/RC, and DIo/RC that correspond to absorption, trapping, and dissipation, respectively. Under CC conditions, in Cd-100 treatment, these parameters increased by 73%, 63%, and 2.3 times (all $p < 0.05$), respectively. Meanwhile, FC increased them by 43%, 44% ($p < 0.05$), and 38% ($p > 0.05$), respectively. Regarding the phenomenological energy fluxes, the most pronounced changes were observed in REo/CSm and RC/CSm, which decreased by 66% and 70% under CC conditions and only 21% and 35% under FC conditions, respectively (all $p < 0.05$). The performance indexes and driving forces changed dramatically under both CC and FC conditions, particularly PItotal and DFtotal. These parameters in Cd-100 treatment were reduced by 87% and 5.0-fold under CC conditions and by 49% and 38% under FC conditions, respectively (all $p < 0.05$) (Fig. 2A, B and Table S5).

Overall, except for Fo, N, REo/RC, DIo/CSm, and REo/CSm, all other JIP-test parameters were significantly affected by Cd. Climate considerably altered Fo, Fv, Fv/Fo, tFm, Area, φPo, φDo, DIo/RC, TRo/CSm, and DIo/CSm. Meanwhile, the interaction of these factors had a significant effect on Fm, Fv, Fv/Fo, Area, Sm, all yield/efficiency parameters, REo/RC, ABS/CSm, TRo/CSm, ETo/CSm, REo/CSm, and performance indexes and driving forces, except SFIabs (Table S4).

3.3. Photosynthetic and antioxidant pigments

Both chlorophylls (Chl) *a* and *b* were significantly influenced by Cd and climate but not their interaction (ANOVA, Table S4). The contents of Chl *a* and *b* were reduced by 37% to 67% ($p < 0.05$) on average in Cd-10–Cd-100 treatments compared to Cd-0 under CC conditions. Under FC conditions, Chl *a* reduced by 38% and 48% ($p < 0.05$) in Cd-50 and Cd-100, and Chl *b* by 20% to 63% ($p < 0.05$) in Cd-10–Cd-100 treatments (Fig. 3A, B). Cd-stressed and non-Cd-affected rapeseed tended to have higher chlorophylls *a* and *b* levels under FC than CC conditions, with Chl *a* content being 45% ($p < 0.05$) higher in Cd-10 treatment and Chl *b* 28% and 35% ($p < 0.05$) in Cd-10 and Cd-50, respectively. Cd significantly affected antioxidant pigments, climate only α-carotene, while the interaction of these factors was substantial only for violaxanthin (Table S4). Contrary to photosynthetic pigments, antioxidant pigments content increased in response to Cd stress (Figs. 3C-G and S1A). The contents of α-carotene, neoxanthin, and violaxanthin were significantly increased in Cd-10–Cd-100 treatments under CC conditions and Cd-50 and Cd-100 under FC. β-carotene content increased considerably in Cd-10–Cd-100 treatments, while lutein content in Cd-50 and Cd-100. Out of these parameters, the most noticeable changes were observed for β-carotene, which increased in stressed plants by 48% to 112% under CC and 40% to 138% under FC conditions, respectively (all $p < 0.05$).

3.4. CBC-related enzymes activity

Cd significantly affected all Calvin-Benson cycle (CBC)-related enzymes, climate RuBisCO, TPI, and PGK activity, and ALS showed factors interaction (Table S4). CBC-related enzyme activity was gradually decreased in response to Cd stress with a higher effect of Cd-10–Cd-100 treatments under CC than FC conditions, except for ALS (Figs. 4A-F and S1A). Under both climates, the most affected enzyme was RuBisCO, which decreased by 60% to 74% in Cd-10–Cd-100 treatments under CC and 17% to 63% in Cd-1–Cd-100 treatments under FC (all $p < 0.05$). RuBisCO, TPI, and PGK activity was consistently higher under FC compared to CC conditions in both non-Cd-affected and Cd-stressed rapeseed, with up to 2.2 and 1.7-fold ($p < 0.05$) for Rubisco and PGK in Cd-50, respectively, and by 2.4-fold ($p < 0.05$) for TPI in Cd-100 (Fig. 4, A, C, D). Meanwhile, the activity of FBPase increased under FC conditions only in Cd-10–Cd-100 treatments, and GAPDH and ALS only in Cd-50 and Cd-100, but did not differ significantly ($p > 0.05$) from those under CC conditions, except that ALS activity of non-Cd-treated rapeseed was by 32% ($p < 0.05$) lower under FC than CC.

3.5. Gas exchange performance

Photosynthetic rate (P_r) and water use efficiency (WUE) of rapeseed grown in low Cd levels did not differ from control (Cd-0), while significantly decreased by 40% and 23% in Cd-50 and by 67% and 60% in Cd-100 treatment, respectively, (all $p < 0.05$) under CC conditions (Figs. 5A, E, and S1A). Under FC conditions, the harmful Cd effect decreased P_r by 13%, 28%, and 58%, and WUE by 10%, 13%, and 34% in Cd-10, Cd-50, and Cd-100 treatments, respectively (all $p < 0.05$). However, in Cd-100, P_r and WUE were 2.3- and 2.8-fold ($p < 0.05$) higher under FC than CC conditions (Fig. 5A, E). In low treatments, Cd did not affect stomatal conductance (g_s) or transpiration rate (E) (Fig. 5B, D). Meanwhile, Cd-50 reduced g_s by 18% ($p < 0.05$) under both climates. It was decreased twice as much as in Cd-50 in Cd-100 under CC ($p < 0.05$) but was less affected under FC conditions (Fig. 5B). E in Cd-50 was reduced by 22% and 17% ($p < 0.05$) under CC and FC, respectively and did not change ($p > 0.05$) between Cd-50 and Cd-100 treatments under CC conditions, while Cd-100 reduced it twice as much as Cd-50 ($p < 0.05$) under FC (Fig. 5D). The intercellular to ambient CO_2 concentration (C_i/C_a) exhibited the opposite response trend to Cd treatment compared to that of P_r under both climates (Figs. 5C and S1A). Under CC conditions, C_i/C_a increased in Cd-50 and Cd-100 by 15% and 26% ($p < 0.05$), respectively, compared to Cd-0. Meanwhile, it started to shift in the reverse direction of P_r in Cd-10 treatment, being 20% ($p < 0.05$) higher in Cd-100 under FC conditions. To sum up, all gas-exchange parameters were considerably affected by Cd. The effect of climate was not substantial for E, while the interaction between these factors on g_s only (Table S4).

3.6. Growth performance

In terms of the onset of visual symptoms of Cd phytotoxicity in the aboveground part, visible leaf lesions such as chlorosis, leaf rolling, and growth retardation were only noticed in plants grown with Cd-50 and Cd-100 treatments, being more pronounced under CC conditions (Fig. 6A and B). Shoot dry weight (DW) of Cd-stressed rapeseed followed the trend of P_r and WUE under both climates (Figs. 6C, 5A, E and S1A). Low soil Cd concentrations did not affect ($p > 0.05$) rapeseed growth under CC conditions. Cd-1 treatment was the only exception, as it had a hormesis effect on root growth, increasing root DW by 38% ($p < 0.05$) compared to control (Cd-0) (Fig. 6C, E). High Cd contamination considerably reduced shoot and root DW by 46% and 58% under Cd-50 and by 68% and 79% under Cd-100 treatment, respectively (all $p < 0.05$). Under FC conditions, a significant reduction of shoot DW started from Cd-10 treatment with 17–53% ($p < 0.05$) decreases under Cd-10−Cd-100 treatments, compared to respective control plants (Cd-0 under FC). Meanwhile, root DW was significantly affected (–42%, $p < 0.05$) only in Cd-100 treatment.

The analysis of two-way ANOVA revealed that both factors (Cd and climate) significantly influenced shoot and root biomass, but the interaction between them was only significant for roots (Table S4). FC conditions improved both non-Cd-affected and Cd-stressed rapeseed growth. Shoot and root DW of rapeseed grown in non-Cd-contaminated soil (Cd-0) under FC increased by 63% and 36% ($p < 0.05$), respectively, compared to CC conditions. Meanwhile, shoot DW of Cd-stressed rapeseed was raised from 32% ($p < 0.05$) under Cd-1 to 2.4-fold ($p < 0.05$) under Cd-100. The stimulating FC effect on root growth was even more pronounced, with root DW being 2.6- and 3.8-fold ($p < 0.05$) higher under FC than CC in Cd-50 and Cd-100 treatments, respectively. However, no significant difference was found between climates regarding root growth in low Cd treatments (Fig. 6C, E).

3.7. Cd concentration in shoots and roots

The Cd concentration in rapeseed increased as soil Cd concentration increased, with roots having significantly higher values than shoots. These increases were considerably reduced under FC compared to CC conditions, especially under high Cd treatments (Figs. 6D, F and S1A). When soil Cd concentration increased from 10 to 100 mg kg^{-1}, Cd concentration in shoots increased nine-fold ($p < 0.05$), reaching the highest values of 106 and 79 μg g^{-1} under CC and FC conditions, respectively. Meanwhile, it raised more than twenty-one and thirteen-fold ($p < 0.05$), reaching 502 and 209 μg g^{-1} in the roots under CC and FC conditions, respectively. Overall, Cd concentration in shoots and roots was significantly influenced by Cd treatment, climate, and Cd × climate interaction (Table S4).

3.8. Phytoextraction efficiency

The tolerance index (TI) of shoots was not affected by low Cd treatments but sharply decreased in Cd-50 and Cd-100 treatments (53% and 32%, $p < 0.05$, respectively), compared to control plants under CC conditions. Meanwhile, TI was significantly but more gradually decreased by Cd-50 and Cd-100 treatments under FC conditions, compared to their respective control, being 40 and 47% ($p < 0.05$) higher under FC than CC conditions (Fig. 6G). Cd translocation from roots to shoots declined with increasing Cd contamination under CC conditions. Meanwhile, no clear TF dependence on Cd soil concentrations was observed under FC. Nevertheless, under both climates, TF values in high Cd treatments were 42% on average ($p < 0.05$) lower than in low Cd treatments (Figs. 6H and S1D). Significant changes between climates in TF were observed only under Cd-100 treatments, i.e., 1.7-fold higher ($p < 0.05$) under FC than CC (Fig. 6H). The bioconcentration factor (BCF) in Cd-contaminated soil was consistently but not significantly lower under FC (0.7–0.9) than in CC (0.9–1.2) conditions ($p > 0.05$). Also, BCF did not differ ($p > 0.05$) between Cd treatments neither under CC nor under FC conditions (Fig. 6I). Contrary to TI, the total Cd uptake (TU) index for shoots increased with increasing soil Cd concentrations under both climates. However, a sharper increase was observed under FC with significantly higher values of TU and potential for Cd phytoextraction in Cd-50 and Cd-100 treatments, compared to CC conditions (Figs. 6J and S1D, Table 1). Therefore, the hypothetical remediation time (HRT) to reduce highly Cd-contaminated soil to the target guideline values was considerably shorter under FC than CC (Table 1). The HRT to Cd pollution limit and lower SGV based on ecological risk under FC would be 48 and 41 years, respectively, in Cd-50 and 82 and 76 years in Cd-100. Meanwhile, an additional 35 or 29 years ($p > 0.05$) in Cd-50 and 61 or 57 years ($p < 0.05$) in Cd-100 would be needed to achieve these goals under CC. According to our results, phytoextraction efficiency-related parameters (TF, TI, TU, and phytoextraction potential) were influenced by Cd, and the effect of Cd was also climate-dependent. Climate significantly affected BCF, TU, and phytoextraction potential (Table S4). Both factors considerably affected HRT but not their interaction.

4. Discussion

4.1. Future climate conditions upregulated the expression of HMA genes involved in Cd translocation in Cd-stressed B. napus

To understand the basis underlying the altered Cd accumulation and translocation under Cd and climate treatment conditions, we evaluated the expression level of genes in the HMA family. These genes play a vital role in Cd transportation and detoxification (Huang et al., 2022; Li et al., 2018; Nazmul Hasan et al., 2022). Previous research has shown that HMA2 and HMA4 are two essential genes that mediate Cd translocation in *Arabidopsis thaliana* (Wong and Cobbett, 2009) and high HMA2 and HMA4 expression in roots is responsible for highly efficient root-to-shoot Cd translocation in *B. napus* (Wu et al., 2015). Although the expression of HMA1-4 genes increased in leaves of *B. napus* grown in high Cd treatments, TF decreased under both CC and FC conditions (Figs. 1A-H, 6H, and S1B). Moreover, the *BnaHMA1a*, *BnaHMA1b*, *BnaHMA2a*, and *BnaHMA4c* genes were significantly negatively correlated with TF ($r = -0.48$ to -0.67, $p < 0.05$). However, in Cd-100 treatment, the expression of *BnaHMA2b*, *BnaHMA3a*, *BnaHMA3b*, and *BnaHMA4a* genes were induced only under FC conditions, and *BnaHMA2a* and *BnaHMA4c* were more expressed under FC than CC (Figs. 1C-H and S1B). Accordingly, cluster analysis group HMA genes in a separate cluster under Cd-100 and FC conditions (Fig. S1B). It suggested that the translocation of Cd from roots to shoots in Cd-100 was enhanced under FC and it well corresponded with the significant increases in TI, TF, and TU index values (Fig. 6G, H, J). Furthermore, a significant positive relationship was found between *BnaHMA3a* and TF ($r = 0.97$, $p < 0.05$), *BnaHMA4a* and *BnaHMA4c* correlated positively with TI ($r = 0.96$ and 0.97, $p < 0.05$), and *BnaHMA4a* with TU ($r = 0.96$, $p < 0.05$). In this regard, different HMA1-4 genes have been reported to be the most important for Cd transportation in rapeseed. For example, the results of Zhang et al. (2020) proposed that *BnaHMA4c* might be the crucial gene for Cd transfer from root to shoot, as its expression level in radicle was significantly higher in Cd-sensitive compared to Cd-tolerant genotype under both normal and Cd stress conditions. They hypothesized that the higher Cd transfer coefficient from radicle to cotyledon might have effectively served the radicle in the Cd-sensitive rapeseed genotype to survive Cd stress with limited detoxification. Meanwhile, Li et al. (2018) found that *BnHMA2;3* likely plays a vital role in Cd influx into the leaves of *B. napus*, as its expression level was the most up-regulated in the leaves of plants treated with Cd. The high expression level of HMA3 in the leaves of Cd hyperaccumulators, such as *T. caerulescens*, also enhanced Cd sequestration into the leaf vacuoles, increasing its uptake (Ueno et al., 2011). However, in Cd non-hyperaccumulator species, Cd is transported to the shoot cells, such as hydathodes and guard cells along the transpiration stream, most likely due to the absence of transporters for accumulation in other leaf cells (Ueno et al., 2011).

4.2. Future climate conditions improved photosynthetic performance in Cd-stressed B. napus

The behavior patterns of JIP-test parameters with the most pronounced peaks in Cd-100 treatment revealed the similar nature of Cd action under both climates. However, it differed notably in extent, with a much higher effect under CC conditions (Fig. 2A, B). The huge increment in dVG/dto and (dV/dt)o in both climates corresponded well with the decreases in tFm, Area, and Sm, exhibiting strong negative linear relationships between them ($r = -0.69$ to -0.91, all $p < 0.001$). The increase in (dV/dt)o implies that the harmful Cd effect caused a higher reduction of Q_A to Q_A^- (i.e., the closure of PSII RCs), converting excitation energy into free energy of the redox couple Q_A^-/Q_A (Strasser et al., 2000). Meanwhile, the decrease in Sm indicated that less energy was required to close all RCs because fewer electrons were transferred into the electron transport chain (ETC) from Q_A^-, resulting in a shorter time to reach the Fm (Strasser et al., 2000). It is reflected by the decline in tFm and its strong positive linear correlation with Sm ($r = 0.77$, $p < 0.001$). Similar behavior of Sm and tFm under Cd stress was observed in the study of Franić et al. (2020). The disturbances in electron transport from RCs to the quinone pool also resulted in a drastic decrease in Area, as previously discussed by other authors (Gautam et al., 2014; Kumar et al., 2020; Mehta et al., 2010). The significant decrease in Fm under CC reflected the increased number of Q_A non-reducing (i.e., non-active) RCs that dissipated the energy of absorbed photons into heat, the process known as non-photochemical quenching (Brestic et al., 2012; Maxwell and Johnson, 2000). As there was no significant change in Fo, Fv also decreased, which in turn resulted in the reduction of Fv/Fo (Fig. 2A and Table S5), indicating a decline in electron supply from the PSII donor side due to functional impairment in the activity of the water-splitting/oxygen-evolving complex (OEC) (Janeeshma et al., 2021). Fm, Fv, and Fv/Fo all had a strong positive linear relationship with Sm (r = 0.81-0.87, $p < 0.001$) under CC conditions.

All the quantum yields related to electron transport were significantly decreased in Cd-100 treatment under CC (Fig. 2A and Table S5) in the sequence φRo > φEo > φPo. This indicated less photoinduced electron transfer from the PSII RC P680 to Q_A, from Q_A^- to PQ, and from PQ^- to PSI end electron acceptors, respectively (Fghire et al., 2015). Therefore, the results imply that Cd affected both the donor and acceptor sides of PSII. It inhibited the OEC on the donor side and electron transport between Q_A^- and Q_B^- (i.e., from primary to secondary quinone electron acceptor of PSII) on the acceptor side, which is consistent with the findings of Sigfridsson et al. (2004) and was previous discussed in our other recent study with rapeseed (Dikšaitytė et al., 2023). Moreover, a reduction in δRo indicates a decrease in electron flow at the acceptor side of PSI caused by the inactivation of ferredoxin-$NADP^+$-reductase (Schansker et al., 2005). Furthermore, unlike the quantum yields associated with electron transport, φDo increased significantly under CC conditions in Cd-100 (Fig. 2A and Table S5), exhibiting a strong negative linear relationship with Fm (r = −0.88, $p < 0.001$). It further suggested that some RCs were transformed into 'heat sinks' where the excitation energy was dissipated as heat rather than being converted to photochemical energy (Strasser et al., 2010).

As the increase in ABS/RC was accompanied by the increases in TRo/RC and DIo/RC (r = 0.99 and 0.96, respectively, $p < 0.001$) and the substantial reduction of RC/ABS (r = −0.96, $p < 0.001$), it indicated changes in both RC functionality and the functional antenna size (Luo et al., 2016; Yusuf et al., 2010). According to Strasser et al. (2000), TRo/RC expresses the initial rate of RCs closure as a fraction of the total number of RCs that can be closed because, under stress conditions, some RCs may be inactivated in the sense of being transformed to quenching sinks without reducing Q_A to Q_A^-. This assumption is supported by the strong positive linear correlation between TRo/RC and (dV/dt)o (r = 0.97,

$p < 0.001$). Meanwhile, like an increase in φDo, an increase in DIo/RC indicates that there were still absorbing antenna Chls that did not feed the active RCs but dissipated their excitation energy through heat (Kalaji et al., 2018; Yusuf et al., 2010). Under both climates, DIo/RC correlated strongly with φDo ($r = 0.92$, $p < 0.001$) and Fm ($r = -0.86$, $p < 0.001$). Furthermore, an increase in TRo/RC, which displayed a strong negative linear relationship with Fv/Fo ($r = -0.94$, $p < 0.001$) under CC, could also be used as an indicator of OEC impairment by stress treatment (Kalaji et al., 2014). In agreement with the finding of Kalaji et al. (2016) that PSII was more sensitive to Cd impact than PSI, the higher increase in TRo/RC than the reduction of quantum yields related to electron transport (Fig. 2A, B and Table S5) indicated that electron flow was most affected at the PSII donor side. Thus, these results suggested that the transformation of some active PSII RCs to non-Q_A-reducing forms could be either due to their structural changes to 'heat sinks' or due to OEC inactivation.

In phenomenological energy fluxes, the ABS/CSm, TRo/CSm, ETo/CSm, and REo/CSm correlated positively with RC/CSm ($r = 0.86-0.95$, $p < 0.001$) and RC/ABS ($r = 0.77-0.86$, $p < 0.001$) and negatively with ABS/RC, TRo/RC, and DIo/RC ($r = -0.78$ to -0.90, $p < 0.001$). ETo/CSm and REo/CSm also exhibited a strong negative linear relationship with (dV/dt)o ($r = -0.95$ and -0.87, respectively, $p < 0.001$). Thus, Cd-induced changes in the specific energy fluxes per active PSII RCs with the reverse response of phenomenological energy fluxes per exited CSm indicated that when a portion of PSII RCs was inactivated, rapeseed leaves adapted to changed RC functionality by enhancing the light energy absorption capacity of the remaining active RCs. These adaptations agree with the findings of other studies (Fghire et al., 2015; Gupta, 2019; Liu et al., 2019).

The decrease in SFIabs suggests that the utilization of absorbed light energy within the remaining active PSII RCs was inefficient due to high dissipation, resulting in the excitation energy not being fully utilized in photochemical reactions. This is supported by a strong negative linear relationship between SFIabs and DIo/RC ($r = -0.89$, $p < 0.001$), which is consistent with the findings of Song et al.

(2016), who demonstrated that with more heat dissipation, the light use efficiency was lower and the reduction in the photosynthetic rate was higher. Therefore, the decline in ETC caused by the loss of PSII activity provides a reasonable explanation of the sharp decrease in PIabs, and the damage to the PSI function perfectly explains the even higher drop in PItotal, which were much more pronounced under CC conditions (Fig. 2A, B and Table S5). As a result, the overall photosynthetic driving forces, DFabs and DFtotal, also fell extremely low. All these performance indexes and driving forces displayed a significant positive linear relationship with P_r (r = 0.48−0.66, $p < 0.001$ or $p < 0.01$).

Cd-induced non-stomatal constraints to photosynthesis could be related to the reduced content of photosynthetic pigments (Fig. 3A, B). Küpper et al. (2007) discovered that cadmium strongly inhibited Chl *a* and *b* synthesis and their stable binding to proteins, causing damage to photosynthetic apparatus, specifically reducing light-harvesting complex II and both photosystems, especially PSII, in both the hyperaccumulator *Thlaspi caerulescens* and the non-accumulator *T. fendleri*. A linear positive relationship between Chl *a* and *b* content and all quantum yields and efficiencies, as well as SFIabs, PIabs, and PItotal, was also found in this study (r = 0.43−0.78, $p < 0.05$). Furthermore, Cd stress decreased the chloroplast density, resulting in chlorosis in rapeseed (Baryla et al., 2001), which was seen in high soil Cd contamination, being more pronounced under CC (Fig. 6A, B). Moreover, the increased content of carotenes and xanthophylls (Fig. 3C-G), which are found in PSII, specifically, β-carotene in RCs while xanthophylls are present in the light-harvesting antenna complexes (Swapnil et al., 2021), could act as the protectors of photosynthetic apparatus against reactive oxygen species (ROS) generation under Cd-10–Cd-100 treatments, as non-enzymatic ROS scavengers (Haider et al., 2021). The protection function has been shown to involve quenching $^3Chl^*$ and $^1O_2$ by excitation transfer mechanism followed by thermal energy dissipation (Swapnil et al., 2021). Correspondingly, a positive correlation was found between these carotenoids (except violaxanthin) and DIo/RC (r = 0.48−0.65, $p < 0.01$), and a negative with Fm (r = −0.40 to −0.57, $p < 0.05$). Meanwhile, φDo had a significant positive correlation with α-carotene (r = 0.49, $p < 0.01$) and lutein (r = 0.36, $p < 0.05$).

Further, the findings of our study revealed that better rapeseed photosynthetic performance under FC in response to Cd stress could also be related to higher enzyme activities related to all carboxylation (RuBisCO), reduction (PGK and GAPDH), and regeneration (FBPase, TPI, and ALS) phases in the C-fixation reactions of photosynthesis (Fig. 4A-F). Cd has previously been shown to inhibit RuBisCO activity in different plant species, such as jack bean (Lee and Roh, 2003) and peppermint (Ahmad et al., 2018). Lee and Roh (2003) discovered that the reduction in RuBisCO activity was related to the decline of RuBisCO activase activity and lower intensity of both the large and small subunits of RuBisCO, leading to a subsequent alteration of RuBisCO levels. In addition, the findings of Song et al. (2019) also suggested that the decrease in photosynthesis caused by Cd exposure may be partly a result of the drop in the values for the maximum rate of RuBisCO carboxylation (V_{cmax}) and ribulose-1,5-bisphosphate (RuBP) regeneration (J_{max}) capacity. Meanwhile, the decline in V_{cmax} could be due to a decrease in active RuBisCO (Peña-Rojas et al., 2004), while J_{max} limited activity of enzymes involved in the regeneration phase of CBC, such as fructose 1,6-bisphosphatase (FBPase) and sedoheptulose-1,7-bisphosphatase (SBPase), and a lack of NADPH or ATP (Lawlor and Cornic, 2002). At photosynthetic machinery, GAPDH and PGK catalyze the reversible conversion of reduction of 3-phosphoglycerate (PGA) to glyceraldehyde-3-phosphate (Michelet et al., 2013; Reddy and Wendisch, 2014), a crucial step in photosynthesis linking the thylakoid membranes' photochemical events with the carbon metabolism (Price et al., 1995). In this study, Rubisco, PGK, GAPDH, FBPase, TPI, and ALS were all significantly positively correlated with all the quantum yields and efficiencies related to electron transport and ETo/CSm (r = 0.36−0.63, $p < 0.05$), except for ALS with φPo. Therefore, these results indicated that Cd threatens to reduce the efficiency of CO_2 fixation, inhibiting the CBC-related enzymes and thus biosynthesis of sucrose and starch, while FC conditions alleviate this treatment. These findings further validated that the effect of Cd stress on rapeseed photosynthesis was mainly non-stomatal limited but caused by the decrease in electron transfer rate.

Moreover, while g_s was significantly decreased in high Cd treatments, C_i/C_a was simultaneously increased under both climate conditions (Fig. 5B, C), showing a strong negative linear correlation (r = −0.88, $p < 0.001$). These results imply higher CO_2 concentration in chloroplasts, which agrees with the effect of Cd shown on CO_2 fixation in different plant species (Andrade et al., 2019; Song et al., 2019; Silva Cunha et al., 2020). Furthermore, C_i/C_a increased more under CC conditions (Fig. 5C), where the lower g_s-induced decrease in CO_2 assimilation potential could not be compensated by higher atmospheric CO_2. This means that non-stomatal Cd constraint was more pronounced under CC, while FC tended to reduce it. In agreement, eCO_2 and temperature were previously found to increase P_r and growth of rapeseed, showing a relatively high upper-temperature rise limit, and eCO_2 further expanded this limit (Dikšaitytė et al., 2020, 2019; Juozapaitienė et al., 2019). The reduction in g_s of Cd-treated rapeseed also correlated well with the response of transpiration (r = 0.90, $p < 0.001$). It has been argued that reduced transpiration in plants exposed to Cd can limit its transport from roots to leaves and thus reduce oxidative damage to the photosynthetic apparatus (Andrade et al., 2019; Gratão et al., 2015). Therefore, it suggested that the decrease in E in high Cd treatments (Fig. 5D) could have been a Cd tolerance strategy to protect photosynthetic functions (Haider et al., 2021) by reducing its translocation from roots to aboveground organs (Fig. 6H). Besides, this assumption corresponds well with the strong positive linear relationship between E and TF (r = 0.77, $p < 0.001$). In addition, E and P_r also had a significant positive linear relationship with WUE (r = 0.48, $p < 0.01$ and r = 0.96, $p < 0.001$, respectively), which measures productivity as an input/output ratio (Evans and Sadler, 2008) and has been defined as the ratio of water used by the plant for metabolism and loss through transpiration (Ruggiero et al., 2017). Thus, the much stronger relationship of WUE to P_r, as compared to E, means that Cd had a significantly higher negative impact on the photosynthesis process than on water balance.

4.3. Climate conditions altered Cd accumulation and phytoextraction efficiency in B. napus

The translocation factor (TF) indicates the plant's efficiency in the transportation of the accumulated metal from its roots to shoots (Ali et al., 2013). It also quantifies plant defense mechanisms that tend to restrict inorganic contaminants to the root system to prevent HM translocation to vital aerial organs (Antoniadis et al., 2017). Our results showed that FC led to increased Cd tolerance of rapeseed grown in Cd-100 treatment (Figs. 6H and S1D), which suggested a more beneficial way for phytoextraction. According to Lux et al. (2004), the tolerance index (TI) > 0.60 indicates high tolerance, 0.60–0.35 – medium, and TI < 0.35 – low tolerance to Cd. Thus, high Cd-50 stress tolerance under FC showed medium acceptance under CC, and low Cd-100 stress tolerance under CC was medium under FC (Figs. 6G and S1D). This is accurate with the onset of visual Cd phytotoxicity symptoms, which were only seen in Cd-50 and Cd-100 treatments and were less pronounced under FC (Fig. 6A and B). TI >1.0 in case of low pollution (as Cd-1 under CC in our case) could be linked to the hormetic effect on the shoot and root growth (Calabrese, 2008). Meanwhile, higher TI values in Cd-50 and Cd-100 under FC (Fig. 6G) corresponded well to lower shoot Cd concentration ($r = -0.89$, $p < 0.01$) due to dilution effect as a result of rapid rapeseed growth (Fig. 6C and E). This explained the increased rapeseed tolerance to Cd under FC conditions (Fig. S1D). In line with these findings, the study of Jia et al. (2010) showed an improvement in Cd tolerance under eCO_2.

Although BCF, as the soil-to-plant index, is closely related to HM's availability to plants (Antoniadis et al., 2017), the lower BCF values under FC than CC (Fig. 6I) hardly reflect a lower Cd availability in this study. Most likely, it is a Cd dilution phenomenon result caused by significantly higher shoot DW under FC (Fig. 6C). This has also led to a considerably higher Cd TU in shoots (Fig. 6J) and thus has enhanced phytoextraction potential under FC compared to CC in high Cd treatments ($p < 0.05$) (Table 1). Therefore, the hypothetical remediation time to reduce heavily Cd-contaminated soil of 100 mg kg^{-1} to the Cd pollution limit of 3 mg kg^{-1} (Dutta et al., 2021) and to lower SGV of 10 mg kg^{-1} based on ecological risk (Tóth et al., 2016) was significantly ($p < 0.05$) shorter under FC compared to CC (Table 1). It can also be seen in a heatmap made of phytoextraction-related parameters and HRT, where Cd-50 and Cd-100 formed separate clusters under CC and FC (Fig. S1D).

4.4. Clustering analysis for B. napus response to Cd under CC and FC

In the hierarchical clustering heatmap (HCA) made of all investigated parameters of rapeseed grown under CC and FC conditions, two clusters for Cd treatments dendrogram were separated. In one of which, low Cd treatments (Cd-1 and Cd-10) were grouped to control plants (Cd-0), while high Cd treatments (Cd-50 and Cd-100) fell into another cluster (Fig. 7). However, Cd-50 in CC and FC conditions made one cluster, while Cd-100 in FC did not cluster together with Cd-100 in CC but it was grouped with Cd-50. Incorporating all the molecular, physiological, biochemical, and growth responses, as well as phytoextraction efficiency, it can be observed that the effect of Cd-100 under FC exhibited greater similarity to Cd-50 effect under both CC and FC than it did with Cd-100 under CC. This pattern is evident in the individual HCAs conducted for parameters related to photosynthetic apparatus performance (Fig. S1C), photosynthetic and antioxidant pigments, CBC-related enzymes, as well as gas exchange and growth parameters (Fig. S1A). In these analyses, Cd-100 treatment under FC was consistently grouped in the same cluster as Cd-50 under CC.

5. Conclusions

Metal transporters, like HMAs, play a vital role in both essential and non-essential metal ion translocation in plants. The analysis of HMA gene expression *in B. napus* in response to different Cd treatments, including low (Cd-1 and Cd-10) and high (Cd-50 and Cd-100) levels of Cd, under both current (CC) and future climate (FC) conditions, demonstrated that when cultivated in soil contaminated with 100 mg kg^{-1} Cd (Cd-100), several HMA genes in *B. napus* leaves exhibited heightened sensitivity to Cd^{2+} ions under FC. According to our study, the higher Cd translocation from roots to leaves was likely due to increased *BnaHMAs,* especially *BnaHMA4a* and *BnaHMA4c*, gene expression. Moreover, high shoot DW accumulation can explain the increase in Cd total uptake (TU) under FC and Cd-100 treatment conditions. Enhanced Cd TU in Cd-50 treatment under FC compared to CC can be mainly attributed to the substantial increase in shoot DW driven by improved photosynthetic performance, particularly in PSII reaction center functionality and CBC-related enzyme activity. Sequentially, this led to hypothetical remediation times that were 35 or 29 years shorter ($p > 0.05$) for reaching the Cd pollution limit of 3 mg kg^{-1} or the lower soil guideline value based on the ecological risk of 10 mg kg^{-1} in Cd-50 and 61 or 57 years shorter ($p < 0.05$) in Cd-100, respectively, under FC compared to CC. Overall, *B. napus* exhibits strong tolerance to low soil Cd contamination in CC and FC conditions, and it demonstrates significant potential for Cd phytoextraction in highly Cd-contaminated soil under FC.

Acknowledgements

This research was funded by the European Social Fund under the No 09.3.3-LMT-K-712 “Development of Competences of Scientists, other Researchers and Students through Practical Research Activities” measure. The authors extend their appreciation to the Researchers Supporting Project number (RSPD2023R725) King Saud University, Riyadh, Saudi Arabia

References

Ahmad, B., Jaleel, H., Sadiq, Y., A. Khan, M.M., Shabbir, A., 2018. Response of exogenous salicylic acid on cadmium induced photosynthetic damage, antioxidant metabolism and essential oil production in peppermint. Plant Growth Regulation 86, 273–286. https://doi.org/10.1007/s10725-018-0427-z

Ali, A., Guo, D., Mahar, A., Ping, W., Wahid, F., Shen, F., Li, R., Zhang, Z., 2017. Phytoextraction and the economic perspective of phytomining of heavy metals. Solid Earth Discussions. https://doi.org/10.5194/se-2017-75

Ali, H., Khan, E., Sajad, M.A., 2013. Phytoremediation of heavy metals—Concepts and applications. Chemosphere 91, 869–881. https://doi.org/10.1016/j.chemosphere.2013.01.075

Andrade, W.V., de Oliveira Neto, C.F., dos Santos Filho, B.G., do Amarante, C.B., Cruz, E.D., Okumura, R.S., Correa Barbosa, A.V., Palheta de Sousa, D.J., Silva Teixeira, J.S., de Santana Botelho, A., 2019. Effect of cadmium on young plants of *Virola surinamensis*. AoB PLANTS 11(3), plz022. https://doi.org/10.1093/aobpla/plz022

Antoniadis, V., Levizou, E., Shaheen, S.M., Ok, Y.S., Sebastian, A., Baum, C., Prasad, M.N.V., Wenzel, W.W., Rinklebe, J., 2017. Trace elements in the soil-plant interface: Phytoavailability, translocation, and phytoremediation–A review. Earth-Science Reviews 171, 621–645. https://doi.org/10.1016/j.earscirev.2017.06.005

Aoyagi, K., Bassham, J.A., 1983. Pyruvate Orthophosphate Dikinase in Wheat Leaves. Plant Physiology 73(3), 853–854. https://doi.org/10.1104/pp.73.3.853

Argüello, J.M., Eren, E., González-Guerrero, M., 2007. The structure and function of heavy metal transport P_{1B}-ATPases. Biometals 20, 233–248. https://doi.org/10.1007/s10534-006-9055-6

Baryla, A., Carrier, P., Franck, F., Coulomb, C., Sahut, C., Havaux, M., 2001. Leaf chlorosis in oilseed rape plants (*Brassica napus*) grown on cadmium-polluted soil: causes and consequences for photosynthesis and growth. Planta 212, 696–709. https://doi.org/10.1007/s004250000439

Bolan, N., Kunhikrishnan, A., Thangarajan, R., Kumpiene, J., Park, J., Makino, T., Kirkham, M.B., Scheckel, K., 2014. Remediation of heavy metal(loid)s contaminated soils – To mobilize or to immobilize? Journal of Hazardous Materials 266, 141–166. https://doi.org/10.1016/j.jhazmat.2013.12.018

Brestic, M., Zivcak, M., Kalaji, H.M., Carpentier, R., Allakhverdiev, S.I., 2012. Photosystem II thermostability in situ: Environmentally induced acclimation and genotype-specific reactions in *Triticum aestivum* L. Plant Physiology and Biochemistry 57, 93–105. https://doi.org/10.1016/j.plaphy.2012.05.012

Calabrese, E.J., 2008. Hormesis: why it is important to toxicology and toxicologists. Environ. Toxicol. Chem. 27(7), 1451–1474. doi: 10.1897/07-541.

Chao, D.-Y., Silva, A., Baxter, I., Huang, Y.S., Nordborg, M., Danku, J., Lahner, B., Yakubova, E., Salt, D.E., 2012. Genome-wide association studies identify heavy metal ATPase3 as the primary determinant of natural variation in leaf cadmium in *Arabidopsis thaliana*. PLoS Genetics 8, e1002923. https://doi.org/10.1371/journal.pgen.1002923

Cojocaru, P., Gusiatin, Z.M., Cretescu, I., 2016. Phytoextraction of Cd and Zn as single or mixed pollutants from soil by rape (*Brassica napus*). Environmental Science and Pollution Research 23, 10693–10701. https://doi.org/10.1007/s11356-016-6176-5

Dan Wang, Heckathorn, S.A., Hamilton, E.W., Frantz, J., 2014. Effects of CO_2 on the tolerance of photosynthesis to heat stress can be affected by photosynthetic pathway and nitrogen. American Journal of Botany 101, 34–44. https://doi.org/10.3732/ajb.1300267

De Sousa, A., AbdElgawad, H., Fidalgo, F., Teixeira, J., Matos, M., Tamagnini, P., Fernandes, R., Figueiredo, F., Azenha, M., Okla, M.K., Teles, L.O., Beemster, G.T.S., Asard, H., 2022. Subcellular compartmentalization of aluminum reduced its hazardous impact on rye photosynthesis. Environmental Pollution 315, 120213. https://doi.org/10.1016/j.envpol.2022.120313

Dikšaitytė, A., Kniuipytė, I., Žaltauskaitė, J., 2023. Drought-free future climate conditions enhance cadmium phytoremediation capacity by *Brassica napus* through improved physiological status. Journal of Hazardous Materials 452, 131181. https://doi.org/10.1016/j.jhazmat.2023.131181

Dikšaitytė, A., Viršilė, A., Žaltauskaitė, J., Januškaitienė, I., Juozapaitienė, G., 2019. Growth and photosynthetic responses in *Brassica napus* differ during stress and recovery periods when exposed to combined heat, drought and elevated CO_2. Plant Physiology and Biochemistry 142, 59–72. https://doi.org/10.1016/j.plaphy.2019.06.026

Dikšaitytė, A., Viršilė, A., Žaltauskaitė, J., Januškaitienė, I., Praspaliauskas, M., Pedišius, N., 2020. Do plants respond and recover from a combination of drought and heatwave in the same manner under adequate and deprived soil nutrient conditions? Plant Science 291, 110333. https://doi.org/10.1016/j.plantsci.2019.110333

Dos Santos Utmazian, M.N., Wieshammer, G., Vega, R., Wenzel, W.W., 2007. Hydroponic screening for metal resistance and accumulation of cadmium and zinc in twenty clones of willows and poplars. Environmental pollution (Barking, Essex : 1987) 148, 155–65. https://doi.org/10.1016/j.envpol.2006.10.045

Dutta, A., Patra, A., Singh Jatav, H., Singh Jatav, S., Kumar Singh, S., Sathyanarayana, E., Verma, S., Singh, P., 2021. Toxicity of cadmium in soil-plant-human continuum and its bioremediation techniques, in: Soil contamination − threats and sustainable solutions. https://doi.org/10.5772/intechopen.94307

Egnér, H., Riehm, H., Domingo, W.R., 1960. Untersuchungen über die chemische bodenanalyse alsgrundlage für die beurteilung des nährstoffzustandes der böden. II. Chemische extraktionsmethoden zur phosphor- und kaliumbestimmung. Kungliga Lantbrukshögskolans Annaler, 26, 199–215.

Esmaeilizadeh, M., Malekzadeh Shamsabad, M.R., Roosta, H.R., Dąbrowski, P., Rapacz, M., Zieliński, A., Wróbel, J., Kalaji, H.M., 2021. Manipulation of light spectrum can improve the performance of photosynthetic apparatus of strawberry plants growing under salt and alkalinity stress. PLOS ONE 16, e0261585. https://doi.org/10.1371/journal.pone.0261585

Evans, R.G., Sadler, E.J., 2008. Methods and technologies to improve efficiency of water use. Water

Resources Research, 44, W00E04. https://doi.org/10.1029/2007WR006200

Fghire, R., Anaya, F., Ali, O.I., Benlhabib, O., Ragab, R., Wahbi, S., 2015. Physiological and photosynthetic response of quinoa to drought stress. Chilean Journal of Agricultural Research 75(2), 174–183. https://doi.org/10.4067/S0718-58392015000200006

Franić, M., Galić, V., Lončarić, Z., Šimić, D., 2020. Genotypic variability of photosynthetic parameters in maize ear-leaves at different cadmium levels in soil. Agronomy 10(7), 986. https://doi.org/10.3390/agronomy10070986

Gallego, S.M., Pena, L.B., Barcia, R.A., Azpilicueta, C.E., Iannone, M.F., Rosales, E.P., Zawoznik, M.S., Groppa, M.D., Benavides, M.P., 2012. Unravelling cadmium toxicity and tolerance in plants: Insight into regulatory mechanisms. Environmental and Experimental Botany 83, 33–46. https://doi.org/10.1016/j.envexpbot.2012.04.006

Gautam, A., Agrawal, D., SaiPrasad, S. V., Jajoo, A., 2014. A quick method to screen high and low yielding wheat cultivars exposed to high temperature. Physiology and Molecular Biology of Plants 20, 533–537. https://doi.org/10.1007/s12298-014-0252-4

Gratão, P.L., Monteiro, C.C., Tezotto, T., Carvalho, R.F., Alves, L.R., Peters, L.P., Azevedo, R.A., 2015. Cadmium stress antioxidant responses and root-to-shoot communication in grafted tomato plants. BioMetals 28, 803–816. https://doi.org/10.1007/s10534-015-9867-3

Guerrieri, R., Belmecheri, S., Ollinger, S. V., Asbjornsen, H., Jennings, K., Xiao, J., Stocker, B.D., Martin, M., Hollinger, D.Y., Bracho-Garrillo, R., Clark, K., Dore, S., Kolb, T., Munger, J.W., Novick, K., Richardson, A.D., 2019. Disentangling the role of photosynthesis and stomatal conductance on rising forest water-use efficiency. Proceedings of the National Academy of Sciences of the United States of America 116, 16909–16914. https://doi.org/10.1073/pnas.1905912116

Guo, H., Zhou, H., Zhang, Y., Du, W., Sun, Y., Yin, Y., Pei, D., Ji, R., Wu, J., Wang, X., Zhu, J., 2015. Combination of elevated CO_2 levels and soil contaminants' stress in wheat and rice, in: Combined stresses in plants. Springer International Publishing, Cham, pp. 71–92. https://doi.org/10.1007/978-3-319-07899-1_4

Guo, H., Zhu, J., Zhou, H., Sun, Y., Yin, Y., Pei, D., Ji, R., Wu, J., Wang, X., 2011. Elevated CO_2 levels affects the concentrations of copper and cadmium in crops grown in soil contaminated with heavy metals under fully open-air field conditions. Environmental Science and Technology 45, 6997–7003. https://doi.org/10.1021/es2001584

Gupta, R., 2019. Tissue specific disruption of photosynthetic electron transport rate in pigeonpea (*Cajanus cajan* L.) under elevated temperature. Plant Signaling & Behavior 14, 1601952. https://doi.org/10.1080/15592324.2019.1601952

Haider, F.U., Liqun, C., Coulter, J.A., Cheema, S.A., Wu, J., Zhang, R., Wenjun, M., Farooq, M., 2021. Cadmium toxicity in plants: Impacts and remediation strategies. Ecotoxicology and Environmental Safety 211, 111887. https://doi.org/10.1016/j.ecoenv.2020.111887

He, S., Yang, X., He, Z., Baligar, V.C., 2017. Morphological and physiological responses of plants to cadmium toxicity: A review. Pedosphere 27, 421–438. https://doi.org/10.1016/S1002-0160(17)60339-4

Huang, C., Picimbon, J.F., Li, H.Q., Li, Z., Liu, Q., Liu, W., 2012. An efficient method for total RNA extraction from peanut seeds. Russian Journal of Plant Physiology 59(1), 129−133. https://doi.org/10.1134/S1021443712010074

Huang, D., Gong, X., Liu, Y., Zeng, G., Lai, C., Bashir, H., Zhou, L., Wang, D., Xu, P., Cheng, M., Wan, J., 2017. Effects of calcium at toxic concentrations of cadmium in plants. Planta 245, 863–873. https://doi.org/10.1007/s00425-017-2664-1

Huang, Q., Qiu, W., Yu, M., Li, S., Lu, Z., Zhu, Y., Kan, X., Zhuo, R., 2022. Genome-wide characterization of *Sedum plumbizincicola* HMA gene family provides functional implications in cadmium response. Plants 11(2): 215. https://doi.org/10.3390/plants11020215

Huang, X.-Y., Deng, F., Yamaji, N., Pinson, S.R.M., Fujii-Kashino, M., Danku, J., Douglas, A., Guerinot, M. Lou, Salt, D.E., Ma, J.F., 2016. A heavy metal P-type ATPase OsHMA4 prevents copper accumulation in rice grain. Nature Communications 7, 12138. https://doi.org/10.1038/ncomms12138

Hussain, B., Ashraf, M.N., Shafeeq-ur-Rahman, Abbas, A., Li, J., Farooq, M., 2021. Cadmium stress in paddy fields: Effects of soil conditions and remediation strategies. Science of The Total Environment 754, 142188. https://doi.org/10.1016/j.scitotenv.2020.142188

Hussain, C.M., Keçili, R., 2020. Environmental pollution and environmental analysis, in: Modern environmental analysis techniques for pollutants. Elsevier, pp. 1–36. https://doi.org/10.1016/B978-0-12-816934-6.00001-1

IPCC, 2021. IPCC: Climate Change 2021: The Physical Science Basis (Summary for Policymakers). Cambridge University Press. In Press.

Janeeshma, E., Kalaji, H.M., Puthur, J.T., 2021. Differential responses in the photosynthetic efficiency of *Oryza sativa* and *Zea mays* on exposure to Cd and Zn toxicity. Acta Physiologiae Plantarum 43: 12. https://doi.org/10.1007/s11738-020-03178-x

Jia, Y., Tang, S., Wang, R., Ju, X., Ding, Y., Tu, S., Smith, D.L., 2010. Effects of elevated CO_2 on growth, photosynthesis, elemental composition, antioxidant level, and phytochelatin concentration in *Lolium mutiforum* and *Lolium perenne* under Cd stress. Journal of Hazardous Materials 180, 384–394. https://doi.org/10.1016/j.jhazmat.2010.04.043

Jiang, Q.-Y., Zhuo, F., Long, S.-H., Zhao, H.-D., Yang, D.-J., Ye, Z.-H., Li, S.-S., Jing, Y.-X., 2016. Can arbuscular mycorrhizal fungi reduce Cd uptake and alleviate Cd toxicity of *Lonicera japonica* grown in Cd-added soils? Scientific Reports 6, 21805. https://doi.org/10.1038/srep21805

Juozapaitienė, G., Dikšaitytė, A., Sujetovienė, G., Aleinikovienė, J., Juknys, R., 2019. Aboveground and below-ground carbon allocation of summer rape under elevated CO_2 and air temperature.

Agricultural and Food Science 28(1), 1–8. https://doi.org/10.23986/afsci.70460

Kalaji, H.M., Jajoo, A., Oukarroum, A., Brestic, M., Zivcak, M., Samborska, I.A., Cetner, M.D., Łukasik, I., Goltsev, V., Ladle, R.J., 2016. Chlorophyll a fluorescence as a tool to monitor physiological status of plants under abiotic stress conditions. Acta Physiologiae Plantarum 38:102. https://doi.org/10.1007/s11738-016-2113-y

Kalaji, H.M., Oukarroum, A., Alexandrov, V., Kouzmanova, M., Brestic, M., Zivcak, M., Samborska, I.A., Cetner, M.D., Allakhverdiev, S.I., Goltsev, V., 2014. Identification of nutrient deficiency in maize and tomato plants by in vivo chlorophyll a fluorescence measurements. Plant Physiology and Biochemistry 81, 16–25. https://doi.org/10.1016/j.plaphy.2014.03.029

Kalaji, H.M., Račková, L., Paganová, V., Swoczyna, T., Rusinowski, S., Sitko, K., 2018. Can chlorophyll-a fluorescence parameters be used as bio-indicators to distinguish between drought and salinity stress in *Tilia cordata* Mill? Environmental and Experimental Botany 152, 149–157. https://doi.org/10.1016/j.envexpbot.2017.11.001

Kniuipytė, I., Dikšaitytė, A., Praspaliauskas, M., Pedišius, N., Žaltauskaitė, J., 2023. Oilseed rape (*Brassica napus* L.) potential to remediate Cd contaminated soil under different soil water content. Journal of Environmental Management 325, 116627. https://doi.org/10.1016/j.jenvman.2022.116627

Kubier, A., Wilkin, R.T., Pichler, T., 2019. Cadmium in soils and groundwater: A review. Applied Geochemistry 108, 104388. https://doi.org/10.1016/j.apgeochem.2019.104388

Khalid, S., Shahid, M., Niazi, N.K., Murtaza, B., Bibi, I., Dumat, C., Khalid, S., Shahid, M., Niazi, N.K., Murtaza, B., Bibi, I., 2017. A comparison of technologies for remediation of heavy metal contaminated soils. Journal of Geochemical Exploration, 182, 247–268. https://doi.org/10.1016/j.gexplo.2016.11.021

Kumar, D., Singh, H., Raj, S., Soni, V., 2020. Chlorophyll a fluorescence kinetics of mung bean (*Vigna* *radiata* L.) grown under artificial continuous light. Biochemistry and Biophysics Reports 24, 100813. https://doi.org/10.1016/j.bbrep.2020.100813

Küpper, H., Parameswaran, A., Leitenmaier, B., Trtílek, M., Šetlík, I., 2007. Cadmium-induced inhibition of photosynthesis and long-term acclimation to cadmium stress in the hyperaccumulator *Thlaspi caerulescens*. New Phytologist 175, 655–674. https://doi.org/10.1111/j.1469-8137.2007.02139.x

Latzko, E., Gibbs, M., 1968. Distribution and activity of enzymes of reductive pentose phosphate cycle in spinach leaves and in chloroplasts isolated by different methods. ZEITSCHRIFT FUR PFLANZENPHYSIOLOGIE 59, 184.

Lawlor, D.W., Cornic, G., 2002. Photosynthetic carbon assimilation and associated metabolism in relation to water deficits in higher plants. Plant, Cell & Environment 25, 275–294. https://doi.org/10.1046/j.0016-8025.2001.00814.x

Lee, K.R., Roh, K.S., 2003. Influence of cadmium on rubisco activation in *Canavalia ensiformis* L. leaves. Biotechnology and Bioprocess Engineering 8, 94–100. https://doi.org/10.1007/BF02940263

Li, N., Xiao, H., Sun, J., Wang, S., Wang, J., Chang, P., Zhou, X., Lei, B., Lu, K., Luo, F., Shi, X., Li, J., 2018. Genome-wide analysis and expression profiling of the HMA gene family in *Brassica napus* under Cd stress. Plant Soil 426, 365–381. https://doi.org/10.1007/s11104-018-3637-2

Li, Y., Zhang, Q., Wang, R., Gou, X., Wang, H., Wang, S., 2012. Temperature changes the dynamics of trace element accumulation in *Solanum tuberosum* L. Climatic Change 112, 655–672. https://doi.org/10.1007/s10584-011-0251-1

Li, Z., Tang, S., Deng, X., Wang, R., Song, Z., 2010. Contrasting effects of elevated CO_2 on Cu and Cd uptake by different rice varieties grown on contaminated soils with two levels of metals: Implication for phytoextraction and food safety. Journal of Hazardous Materials 177, 352–361. https://doi.org/10.1016/j.jhazmat.2009.12.039

Lindsey, R., 2022. Climate change: atmospheric carbon dioxide. NOAA Clim. 2022, 1–5.

Liu, X., Zhang, H., Wang, J., Wu, X., Ma, S., Xu, Z., Zhou, T., Xu, N., Tang, X., An, B., 2019. Increased CO_2 concentrations increasing water use efficiency and improvement PSII function of mulberry seedling leaves under drought stress. Journal of Plant Interactions 14(1), 213–223. https://doi.org/10.1080/17429145.2019.1603405

Luo, H.H., Merope, T.M., Zhang, Y.L., Zhang, W.F., 2016. Combining gas exchange and chlorophyll a fluorescence measurements to analyze the photosynthetic activity of drip-irrigated cotton under different soil water deficits. Journal of Integrative Agriculture 15(6), 1256–1266. https://doi.org/10.1016/S2095-3119(15)61270-9

Lux, A., Sottnikova, A., Opatrna, J., Greger, M., 2004. Differences in structure of adventitious roots in *Salix* clones with contrasting characteristics of cadmium accumulation and sensitivity. Physiologia Plantarum 120, 537–545. https://doi.org/10.1111/j.0031-9317.2004.0275.x

Ma, N., Wang, W., Gao, J., Chen, J., 2017. Removal of cadmium in subsurface vertical flow constructed wetlands planted with *Iris sibirica* in the low-temperature season 109, 48–56. Ecological Engineering. https://doi.org/10.1016/j.ecoleng.2017.09.008

Maxwell, K., Johnson, G.N., 2000. Chlorophyll fluorescence—a practical guide. Journal of Experimental Botany 51, 659–668. https://doi.org/10.1093/jxb/51.345.659

Mehta, P., Jajoo, A., Mathur, S., Bharti, S., 2010. Chlorophyll a fluorescence study revealing effects of high salt stress on Photosystem II in wheat leaves. Plant Physiology and Biochemistry 48, 16–20. https://doi.org/10.1016/j.plaphy.2009.10.006

Michelet, L., Zaffagnini, M., Morisse, S., Sparla, F., Pérez-Pérez, M.E., Francia, F., Danon, A., Marchand, C.H., Fermani, S., Trost, P., Lemaire, S.D., 2013. Redox regulation of the Calvin-Benson cycle: Something old, something new. Frontiers in Plant Science 4, 470. https://doi.org/10.3389/fpls.2013.00470

Mikkelsen, M.D., Pedas, P., Schiller, M., Vincze, E., Mills, R.F., Borg, S., Møller, A., Schjoerring, J.K., Williams, L.E., Baekgaard, L., Holm, P.B., Palmgren, M.G., 2012. Barley HvHMA1 is a heavy metal pump involved in mobilizing organellar Zn and Cu and plays a role in metal loading into grains. PLoS One 7, e49027. https://doi.org/10.1371/journal.pone.0049027

Mohabubul Haque, A.F.M., Gohari, G., El-Shehawi, A.M., Dutta, A.K., Elseehy, M.M., Kabir, A.H., 2022. Genome-wide identification, characterization and expression profiles of heavy metal ATPase 3 (HMA3) in plants. Journal of King Saud University - Science 34(1), 101730. https://doi.org/10.1016/j.jksus.2021.101730

Morel, M., Crouzet, J., Gravot, A., Auroy, P., Leonhardt, N., Vavasseur, A., Richaud, P., 2009. AtHMA3, a P_{1B}-ATPase allowing Cd/Zn/Co/Pb vacuolar storage in Arabidopsis. Plant Physiology 149(2), 894–904. https://doi.org/10.1104/pp.108.130294

Nazmul Hasan, M., Islam, S., Bhuiyan, F.H., Arefin, S., Hoque, H., Azad Jewel, N., Ghosh, A., Prodhan, S.H., 2022. Genome wide analysis of the heavy-metal-associated (HMA) gene family in tomato and expression profiles under different stresses. Gene 835: 146664. https://doi.org/10.1016/j.gene.2022.146664

Noyes, P.D., McElwee, M.K., Miller, H.D., Clark, B.W., Van, Tiem, L.A., Walcott, K.C., Erwin, K.N., Levin, E.D., 2009. The toxicology of climate change: Environmental contaminants in a warming world. Environment International 35(6), 971–986. https://doi.org/10.1016/j.envint.2009.02.006

Peña-Rojas, K., Aranda, X., Fleck, I., 2004. Stomatal limitation to CO_2 assimilation and down-regulation of photosynthesis in *Quercus ilex* resprouts in response to slowly imposed drought. Tree Physiology 24, 813–22. https://doi.org/10.1093/treephys/24.7.813

Pourghasemian, N., Ehsanzadeh, P., Greger, M., 2013. Genotypic variation in safflower (*Carthamus* spp.) cadmium accumulation and tolerance affected by temperature and cadmium levels. Environmental and Experimental Botany 87, 218–226.

https://doi.org/10.1016/j.envexpbot.2012.12.003

Price, G.D., Evans, J.R., von Caemmerer, S., Yu, J.-W., Badger, M.R., 1995. Specific reduction of chloroplast glyceraldehyde-3-phosphate dehydrogenase activity by antisense RNA reduces CO_2 assimilation via a reduction in ribulose bisphosphate regeneration in transgenic tobacco plants. Planta 195, 369–378. https://doi.org/10.1007/BF00202594

Rabêlo, F.H.S., Borgo, L., Merloti, L.F., Pylro, V.S., Navarrete, A.A., Mano, R.H., Thijs, S., Vangronsveld, J., Alleoni, L.R.F., 2020. Effects of winter and summer conditions on Cd fractionation and bioavailability, bacterial communities and Cd phytoextraction potential of *Brachiaria decumbens* and *Panicum maximum* grown in a tropical soil. Science of The Total Environment 728, 138885. https://doi.org/10.1016/j.scitotenv.2020.138885

Racker, E., 1962. [29a] Ribulose diphosphate carboxylase from spinach leaves. Ribulose diphosphate+CO_2+H_2O→2 3-P-Glycerate. Methods Enzymology 5, 266–270. https://doi.org/10.1016/S0076-6879(62)05216-7

Rajkumar, M., Prasad, M.N.V., Swaminathan, S., Freitas, H., 2013. Climate change driven plant–metal–microbe interactions. Environment International 53, 74–86. https://doi.org/10.1016/j.envint.2012.12.009

Reddy, G., Wendisch, V.F., 2014. Characterization of 3-phosphoglycerate kinase from *Corynebacterium glutamicum* and its impact on amino acid production. BMC Microbiology 14: 54. https://doi.org/10.1186/1471-2180-14-54

Reimann, C., Fabian, K., Birke, M., Filzmoser, P., Demetriades, A., Négrel, P., Oorts, K., Matschullat, J., de Caritat, P., Albanese, S., Anderson, M., Baritz, R., Batista, M.J., Bel-Ian, A., Cicchella, D., De Vivo, B., De Vos, W., Dinelli, E., Ďuriš, M., Dusza-Dobek, A., Eggen, O.A., Eklund, M., Ernsten, V., Flight, D.M.A., Forrester, S., Fügedi, U., Gilucis, A., Gosar, M., Gregorauskiene, V., De Groot, W., Gulan, A., Halamić, J., Haslinger, E., Hayoz, P., Hoogewerff, J., Hrvatovic, H., Husnjak, S., Jähne-Klingberg, F., Janik, L., Jordan, G., Kaminari, M., Kirby, J., Klos, V., Kwećko, P., Kuti, L., Ladenberger, A., Lima, A., Locutura, J., Lucivjansky, P., Mann, A., Mackovych, D., McLaughlin, M., Malyuk, B.I., Maquil, R., Meuli, R.G., Mol, G., O'Connor, P., Ottesen, R.T., Pasnieczna, A., Petersell, V., Pfleiderer, S., Poňavič, M., Prazeres, C., Radusinović, S., Rauch, U., Salpeteur, I., Scanlon, R., Schedl, A., Scheib, A., Schoeters, I., Šefčik, P., Sellersjö, E., Slaninka, I., Soriano-Disla, J.M., Šorša, A., Svrkota, R., Stafilov, T., Tarvainen, T., Tendavilov, V., Valera, P., Verougstraete, V., Vidojević, D., Zissimos, A., Zomeni, Z., Sadeghi, M., 2018. GEMAS: Establishing geochemical background and threshold for 53 chemical elements in European agricultural soil. Applied Geochemistry. https://doi.org/10.1016/j.apgeochem.2017.01.021

Rizwan, M., Ali, S., Zia Ur Rehman, M., Rinklebe, J., Tsang, D.C.W., Bashir, A., Maqbool, A., Tack, F.M.G., Ok, Y.S., 2018. Cadmium phytoremediation potential of *Brassica* crop species: A review. Science of The Total Environment 631–632, 1175–1191. https://doi.org/10.1016/j.scitotenv.2018.03.104

Rodriguez, J.H., Klumpp, A., Fangmeier, A., Pignata, M.L., 2011. Effects of elevated CO_2 concentrations and fly ash amended soils on trace element accumulation and translocation among roots, stems and seeds of *Glycine max* (L.) Merr. Journal of Hazardous Materials 187, 58–66. https://doi.org/10.1016/j.jhazmat.2010.11.068

Romih, N., Grabner, B., Lakota, M., Ribarič-Lasnik, C., 2012. Distribution of Cd, Pb, Zn, Mo, and S in juvenile and mature *Brassica napus* L. var. napus. International Journal of Phytoremediation 14, 282–301. https://doi.org/10.1080/15226514.2010.549859

Ruggiero, A., Punzo, P., Landi, S., Costa, A., Van Oosten, M.J., Grillo, S., 2017. Improving plant water use efficiency through molecular genetics. Horticulturae 3(2), 31. https://doi.org/10.3390/horticulturae3020031

Russell, G.K., Gibbs, M., 1967. Partial purification and characterization of two fructose diphosphate aldolases from *Chlamydomonas mundana*. Biochimica et Biophysica Acta (BBA) - Enzymology 132, 145–154. https://doi.org/10.1016/0005-2744(67)90200-8

Sabir, A., Naveed, M., Bashir, M.A., Hussain, A., Mustafa, A., Zahir, Z.A., Kamran, M., Ditta, A., Núñez-Delgado, A., Saeed, Q., Qadeer, A., 2020. Cadmium mediated phytotoxic impacts in *Brassica napus*: Managing growth, physiological and oxidative disturbances through combined use of biochar and *Enterobacter* sp. MN17. Journal of Environmental Management 265, 110522. https://doi.org/10.1016/j.jenvman.2020.110522

Samborska, I.A., Kalaji, H.M., Sieczko, L., Borucki, W., Mazur, R., Kouzmanova, M., Goltsev, V., 2019. Can just one-second measurement of chlorophyll a fluorescence be used to predict sulphur deficiency in radish (*Raphanus sativus* L. *sativus*) plants? Current Plant Biology 19, 100096. https://doi.org/10.1016/j.cpb.2018.12.002

Schansker, G., Tóth, S.Z., Strasser, R.J., 2005. Methylviologen and dibromothymoquinone treatments of pea leaves reveal the role of photosystem I in the Chl a fluorescence rise OJIP. Biochimica et Biophysica Acta (BBA) - Bioenergetics 1706, 250–261. https://doi.org/10.1016/j.bbabio.2004.11.006

Sebastian, A., Prasad, M.N.V., 2014. Cadmium minimization in rice. A review. Agronomy for Sustainable Development 34, 155–173. https://doi.org/10.1007/s13593-013-0152-y

Sigfridsson, K.G.V., Bernát, G., Mamedov, F., Styring, S., 2004. Molecular interference of Cd^{2+} with Photosystem II. Biochimica et Biophysica Acta (BBA) - Bioenergetics 1659, 19–31. https://doi.org/10.1016/j.bbabio.2004.07.003

Silva Cunha, L.F., Oliveira, V.P., Nascimento, A.W.S., Silva, B.R.S., Batista, B.L., Alsahli, A.A., Lobato, A.K. da S., 2020. Leaf application of 24-epibrassinolide mitigates cadmium toxicity in young *Eucalyptus urophylla* plants by modulating leaf anatomy and gas exchange. Physiologia Plantarum 173(1), 67–87. https://doi.org/10.1111/ppl.13182

Soares, C., de Sousa, A., Pinto, A., Azenha, M., Teixeira, J., Azevedo, R.A., Fidalgo, F., 2016. Effect of 24-epibrassinolide on ROS content, antioxidant system, lipid peroxidation and Ni uptake in *Solanum nigrum* L. under Ni stress. Environmental and Experimentaly Botany 122, 115–125. https://doi.org/10.1016/j.envexpbot.2015.09.010

Song, X., Yue, X., Chen, W., Jiang, H., Han, Y., Li, X., 2019. Detection of cadmium risk to the photosynthetic performance of *Hybrid pennisetum*. Frontiers in Plant Science 10:798. https://doi.org/10.3389/fpls.2019.00798

Song, X., Zhou, G., Xu, Z., Lv, X., Wang, Y., 2016. A self-photoprotection mechanism helps *Stipa baicalensis* adapt to future climate change. Scientific Reports 6: 25839. https://doi.org/10.1038/srep25839

Stirbet, A., Govindjee, 2011. On the relation between the Kautsky effect (chlorophyll *a* fluorescence induction) and Photosystem II: basics and applications of the OJIP fluorescence transient. Journal of Photochemistry and Photobiology B: Biology 104(1-2), 236–257. https://doi.org/10.1016/j.jphotobiol.2010.12.010

Stirbet, A., Lazár, D., Kromdijk, J., Govindjee, 2018. Chlorophyll *a* fluorescence induction: can just a one-second measurement be used to quantify abiotic stress responses? Photosynthetica 56, 86–104. https://doi.org/10.1007/s11099-018-0770-3

Strasser, R.J., Srivastava, A., Tsimilli-Michael, M., 2000. The fluorescence transient as a tool to characterize and screen photosynthetic samples. Probing Photosynthesis: Mechanism, Regulation & Adaptation.

Strasser, R.J., Tsimilli-Michael, M., Qiang, S., Goltsev, V., 2010. Simultaneous in vivo recording of prompt and delayed fluorescence and 820 nm reflection changes during drying and after rehydration of the resurrection plant *Haberlea rhodopensis*. Biochimica et Biophysica Acta (BBA) - Bioenergetics 1797(6-7), 1313–1326. https://doi.org/10.1016/j.bbabio.2010.04.365

Strasser, R.J., Tsimilli-Michael, M., Srivastava, A., 2004. Analysis of the Chlorophyll *a* Fluorescence Transient. pp. 321–362. https://doi.org/10.1007/978-1-4020-3218-9_12

Suman, J., Uhlik, O., Viktorova, J., Macek, T., 2018. Phytoextraction of heavy metals: a promising tool for clean-up of polluted environment? Frontiers in Plant Science 9:1476. https://doi.org/10.3389/fpls.2018.01476

Swapnil, P., Meena, M., Singh, S.K., Dhuldhaj, U.P., Harish, Marwal, A., 2021. Vital roles of carotenoids in plants and humans to deteriorate stress with its structure, biosynthesis, metabolic engineering and functional aspects. Current Plant Biology 26, 100203. https://doi.org/10.1016/j.cpb.2021.100203

Tan, J., Wang, J., Chai, T., Zhang, Y., Feng, S., Li, Y., Zhao, H., Liu, H., Chai, X., 2013. Functional analyses of TaHMA2, a P_{1B} -type ATPase in wheat. Plant Biotechnology Journal 11, 420–431. https://doi.org/10.1111/pbi.12027

Tebaldi, C., Debeire, K., Eyring, V., Fischer, E., Fyfe, J., Friedlingstein, P., Knutti, R., Lowe, J., O'Neill, B., Sanderson, B., van Vuuren, D., Riahi, K., Meinshausen, M., Nicholls, Z., Tokarska, K.B., Hurtt, G., Kriegler, E., Lamarque, J.-F., Meehl, G., Moss, R., Bauer, S.E., Boucher, O., Brovkin, V., Byun, Y.-H., Dix, M., Gualdi, S., Guo, H., John, J.G., Kharin, S., Kim, Y., Koshiro, T., Ma, L., Olivié, D., Panickal, S., Qiao, F., Rong, X., Rosenbloom, N., Schupfner, M., Séférian, R., Sellar, A., Semmler, T., Shi, X., Song, Z., Steger, C., Stouffer, R., Swart, N., Tachiiri, K., Tang, Q., Tatebe, H., Voldoire, A., Volodin, E., Wyser, K., Xin, X., Yang, S., Yu, Y., Ziehn, T., 2021. Climate model projections from the Scenario Model Intercomparison Project (ScenarioMIP) of CMIP6. Earth Syst. Dyn. 12, 253–293. https://doi.org/10.5194/esd-12-253-2021

Tóth, G., Hermann, T., Da Silva, M.R., Montanarella, L., 2016. Heavy metals in agricultural soils of the European Union with implications for food safety. Environment international 88, 299–309. https://doi.org/10.1016/j.envint.2015.12.017

Ueno, D., Milner, M.J., Yamaji, N., Yokosho, K., Koyama, E., Clemencia Zambrano, M., Kaskie, M., Ebbs, S., Kochian, L. V., Ma, J.F., 2011. Elevated expression of TcHMA3 plays a key role in the extreme Cd tolerance in a Cd-hyperaccumulating ecotype of *Thlaspi caerulescens*. The Plant Journal 66, 852–862. https://doi.org/10.1111/j.1365-313X.2011.04548.x

Ueno, D., Yamaji, N., Kono, I., Huang, C.F., Ando, T., Yano, M., Ma, J.F., 2010. Gene limiting cadmium accumulation in rice. Proceedings of the National Academy of Sciences (PNAS) 107(38), 16500–16505. https://doi.org/10.1073/pnas.1005396107

Wang, Z.Y., Portis, A.R., 1992. Dissociation of ribulose-1,5-bisphosphate bound to ribulose-1,5-bisphosphate carboxylase/oxygenase and its enhancement by ribulose-1,5-bisphosphate carboxylase/oxygenase activase-mediated hydrolysis of ATP. Plant Physiology 99(4), 1348–1353 https://doi.org/10.1104/pp.99.4.1348

Wheal, M.S., Fowles, T.O., Palmer, L.T., 2011. A cost-effective acid digestion method using closed polypropylene tubes for inductively coupled plasma optical emission spectrometry (ICP-OES) analysis of plant essential elements. Analytical Methods 3(12), 2854–2863. https://doi.org/10.1039/c1ay05430a

Wong, C.K.E., Cobbett, C.S., 2009. HMA P-type ATPases are the major mechanism for root-to-shoot Cd translocation in *Arabidopsis thaliana*. New Phytologist 181, 71–78. https://doi.org/10.1111/j.1469-8137.2008.02638.x

World Meteorological Organization (WMO). 2022. *State of the Climate in Europe 2021* (WMO-No. 1304). Geneva.

Wu, Z., Zhao, X., Sun, X., Tan, Q., Tang, Y., Nie, Z., Hu, C., 2015. Xylem transport and gene expression play decisive roles in cadmium accumulation in shoots of two oilseed rape cultivars (*Brassica napus*). Chemosphere 119, 1217–1223. https://doi.org/10.1016/j.chemosphere.2014.09.099

Yamaji, N., Xia, J., Mitani-Ueno, N., Yokosho, K., Feng Ma, J., 2013. Preferential delivery of Zinc to developing tissues in rice is mediated by P-type heavy metal ATPase OsHMA2. Plant Physiology

162(2), 927–939. https://doi.org/10.1104/pp.113.216564

Yan, A., Wang, Y., Tan, S.N., Mohd Yusof, M.L., Ghosh, S., Chen, Z., 2020. Phytoremediation: A promising approach for revegetation of heavy metal-polluted land. Frontiers in Plant Science 11:359. https://doi.org/10.3389/fpls.2020.00359

Yang, Y., Ge, Y., Zeng, H., Zhou, X., Peng, L., Zeng, Q., 2017. Phytoextraction of cadmium-contaminated soil and potential of regenerated tobacco biomass for recovery of cadmium. Scientific Reports 7: 7210. https://doi.org/10.1038/s41598-017-05834-8

Yusuf, M.A., Kumar, D., Rajwanshi, R., Strasser, R.J., Tsimilli-Michael, M., Govindjee, Sarin, N.B., 2010. Overexpression of γ-tocopherol methyl transferase gene in transgenic *Brassica juncea* plants alleviates abiotic stress: Physiological and chlorophyll *a* fluorescence measurements. Biochimica et Biophysica Acta (BBA) - Bioenergetics 1797, 1428–1438. https://doi.org/10.1016/j.bbabio.2010.02.002

Zhang, F., Xiao, X., Yan, G., Hu, J., Cheng, X., Li, L., Li, H., Wu, X., 2018. Association mapping of cadmium-tolerant QTLs in *Brassica napus* L. and insight into their contributions to phytoremediation. Environmental and Experimentaly Botany 155, 420–428. https://doi.org/10.1016/j.envexpbot.2018.07.014

Zhang, F., Xiao, X., Wu, X., 2020. Physiological and molecular mechanism of cadmium (Cd) tolerance at initial growth stage in rapeseed (*Brassica napus* L.). Ecotoxicology and Environmental Safety 197: 110613. https://doi.org/10.1016/j.ecoenv.2020.110613

Zheng, J., Wang, H., Li, Z., Tang, S., Chen, Z., 2008. Using elevated carbon dioxide to enhance copper accumulation in *Pteridium revolutum*, a copper-tolerant plant, under experimental conditions. International Journal of Phytoremediation 10, 161–172. https://doi.org/10.1080/15226510801913934

Table 1. Cd phytoextraction potential in Cd-1–Cd-100 treatments under CC (21/14 °C, 400 ppm) and FC (25/18 °C, 800 ppm) conditions and hypothetical remediation time required to reduce the soil Cd concentration from 10–100 mg kg^{-1} to 3 mg kg^{-1} (Cd pollution limit (Dutta et al., 2021; Reimann et al., 2018) and SGV for Lithuania (Reimann et al., 2018)) and from 50–100 mg kg^{-1} to 10 mg kg^{-1} (lower SGV based on ecological risk) (Tóth et al., 2016). Different letters next to the values indicate significant differences among the treatments according to Fischer's LSD ($p \leq 0.05$).

Soil Cd pollution	Cd phytoextraction potential (kg ha^{-1} year^{-1})		Hypothetical remediation time (years)			
			to pollution limit (3 mg kg^{-1})		to lower SGV (10 mg kg^{-1}) (e)*	
	CC	FC	CC	FC	CC	FC
Cd-1	0.035 ± 0.002^{c}	0.037 ± 0.008^{c}				
Cd-10	0.385 ± 0.036^{c}	0.431 ± 0.028^{c}	33 ± 3^{c}	29 ± 2^{c}		
Cd-50	1.075 ± 0.230^{b}	1.771 ± 0.012^{a}	83 ± 18^{b}	48 ± 0^{bc}	70 ± 15^{b}	41 ± 0^{b}
Cd-100	1.239 ± 0.164^{b}	2.186 ± 0.332^{a}	143 ± 19^{a}	82 ± 12^{b}	133 ± 18^{a}	76 ± 12^{b}

Assumptions made for the calculation: i) the total soil Cd concentration decreases linearly because of a constant yearly extraction and ii) a depth of the arable layer (or pollution depth) is 0.15 m. * – '(e)' means that the guideline value has been defined on the basis of ecological risk

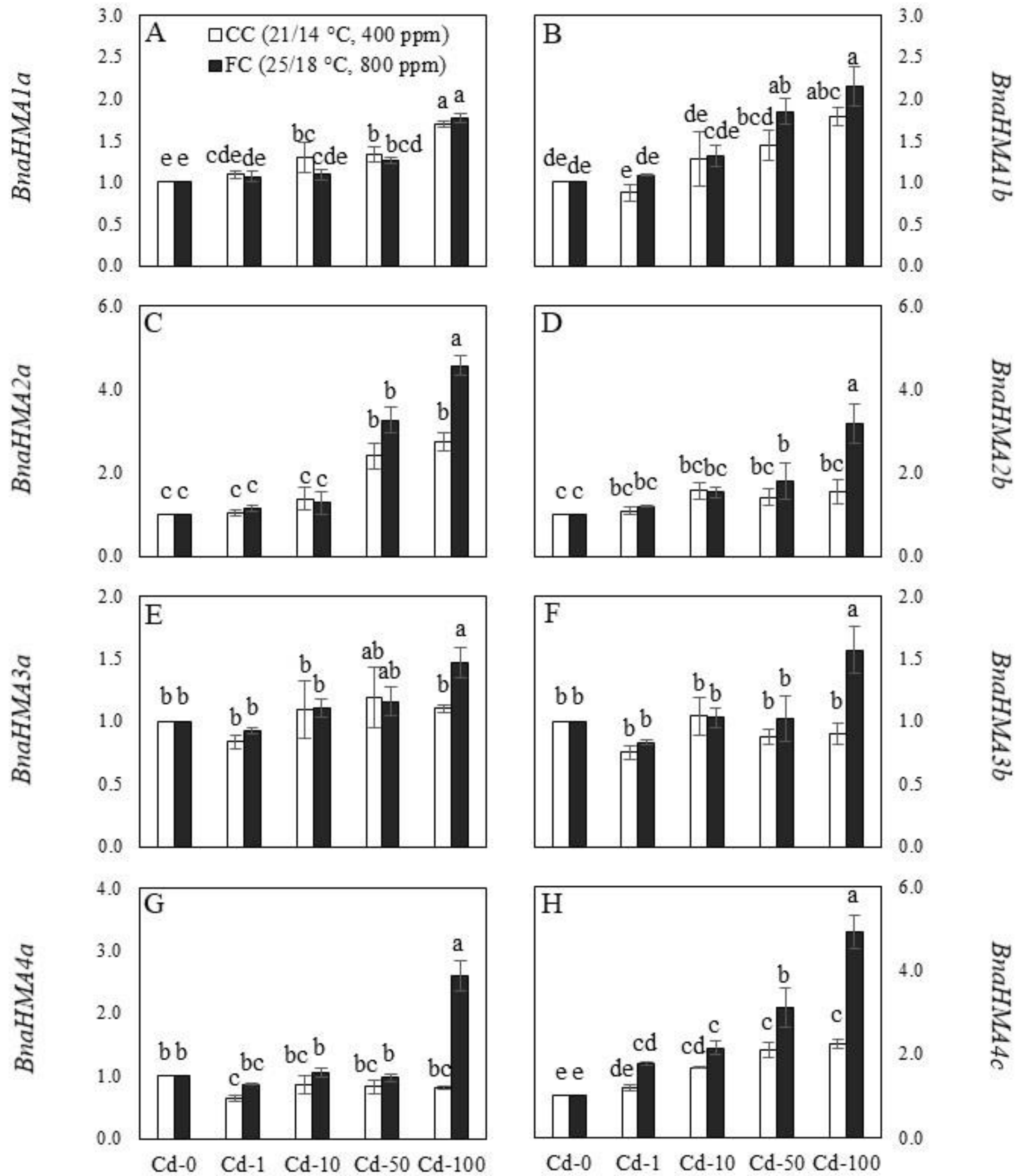

Fig. 1. Relative expression levels of eight heavy metal ATPases (*HMAs*) genes in rapeseed (*Brassica napus*) exposed to Cd treatments (Cd-0, Cd-1, Cd-10, Cd-50, and Cd-100) under current climate (CC) and future climate (FC) conditions. Vertical bars represent ± SE of the mean ($n = 3$). Under both climate conditions, the expression levels of HMA genes in Cd-stressed rapeseed (Cd-1, Cd-10, Cd-50, and Cd-100) are shown relative to the expression levels of HMA genes in control, i.e., Cd-untreated ones (Cd-0), set to 1. Different letters indicate significant differences among the treatments according to Fischer's LSD ($p \leq 0.05$).

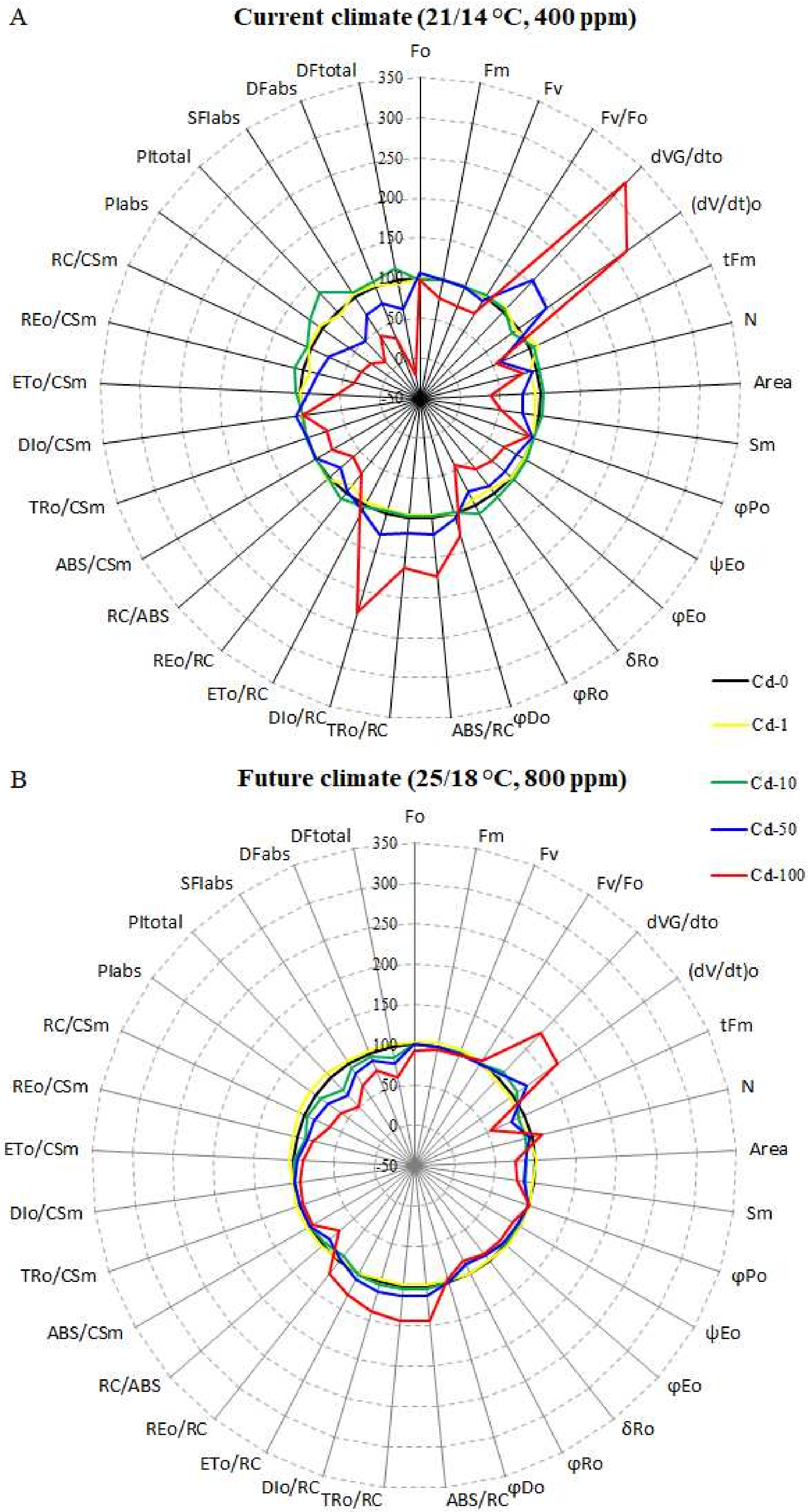
A
Current climate (21/14 °C, 400 ppm)
B
Future climate (25/18 °C, 800 ppm)
Fo
Fm
Fv
Fv/Fo
dVG/dto
(dV/dt)o
tFm
N
Area
Sm
φPo
ψEo
φEo
δRo
φRo
φDo
ABS/RC
TRo/RC
DIo/RC
ETo/RC
REo/RC
RC/ABS
ABS/CSm
TRo/CSm
DIo/CSm
ETo/CSm
REo/CSm
RC/CSm
PIabs
PItotal
SFIabs
DFabs
DFtotal
350
300
250
200
150
100
50
0
-50
Cd-0
Cd-1
Cd-10
Cd-50
Cd-100

Fig. 2. JIP-test parameters normalized on radar plots. [A] The effect of cadmium (Cd) under current climate conditions; [B] the effect of cadmium (Cd) under future climate conditions. Each curve represents the average of 3 measurements per treatment. Under both climate conditions, the status of Cd-stressed rapeseed (Cd-1, Cd-10, Cd-50, and Cd-100) is shown relative to the status of control, i.e., Cd-untreated ones (Cd-0), expressed as 100% (*black line*).

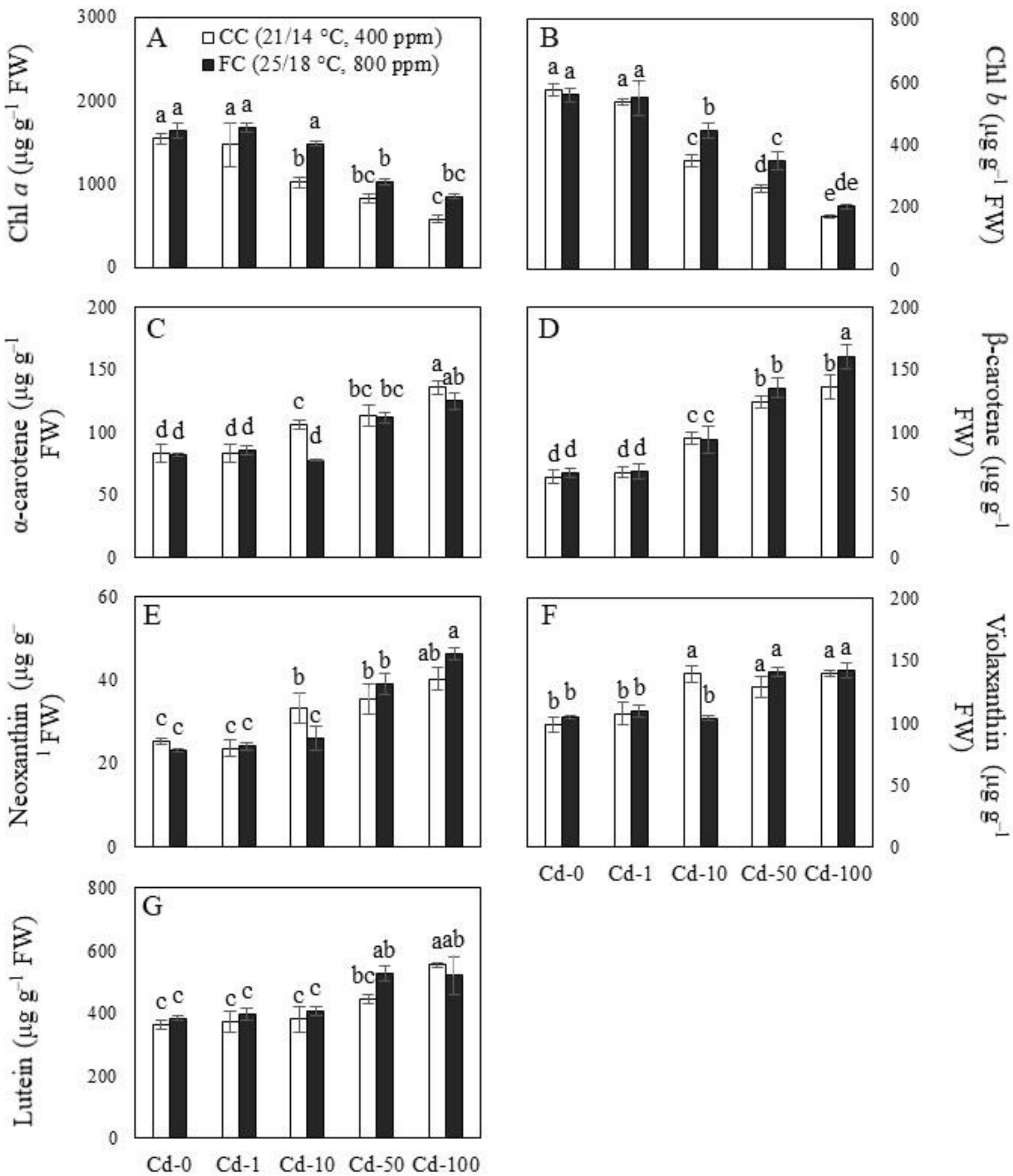

Fig. 3. Photosynthetic and antioxidant pigments content in rapeseed (*Brassica napus*) exposed to Cd treatments (Cd-0, Cd-1, Cd-10, Cd-50, and Cd-100) under current climate (CC) and future climate (FC) conditions. [A] Chlorophyll *a* (Chl *a*); [B] Chlorophyll *b* (Chl *b*); [C] α-carotene; [D] β-carotene; [E] Neoxanthin; [F] Violaxanthin; [G] Lutein. Vertical bars represent ± SE of the mean (n = 3); Different letters indicate significant differences among the treatments according to Fischer's LSD ($p \leq 0.05$).

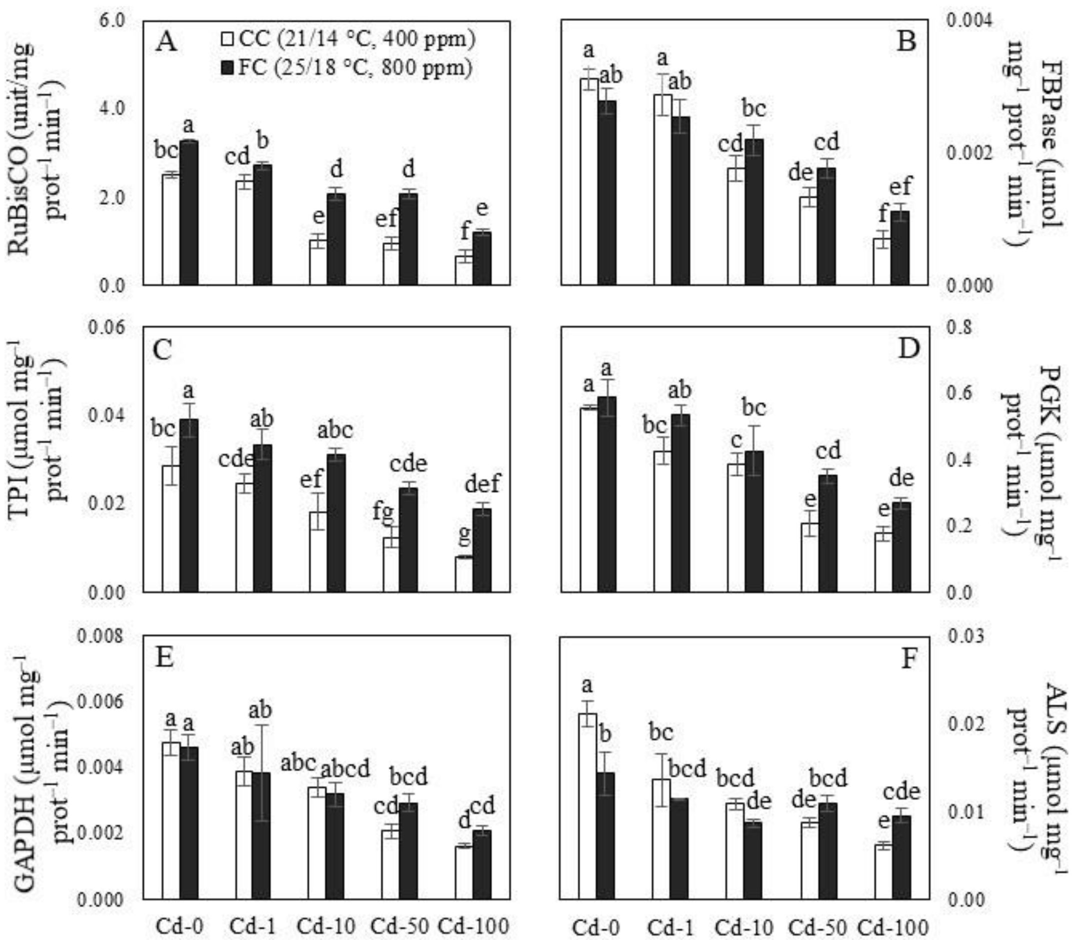

Fig. 4. Calvin cycle-related enzymes activity in rapeseed (*Brassica napus*) exposed to Cd treatments (Cd-0, Cd-1, Cd-10, Cd-50, and Cd-100) under current climate (CC) and future climate (FC) conditions. [A] Ribulose 1,5-bisphosphate carboxylase/oxygenase (RuBisCO); [B] Fructose 1,6-bisphosphatase (FBPase); [C] Triosephosphate isomerase (TPI); [D] Phosphoglycerate kinase (PGK); [E]

Glyceraldehyde 3-phosphate dehydrogenase (GAPDH); [F] Aldolase (ALS). Vertical bars represent ± SE of the mean ($n = 3$); Different letters indicate significant differences among the treatments according to Fischer's LSD ($p \leq 0.05$).

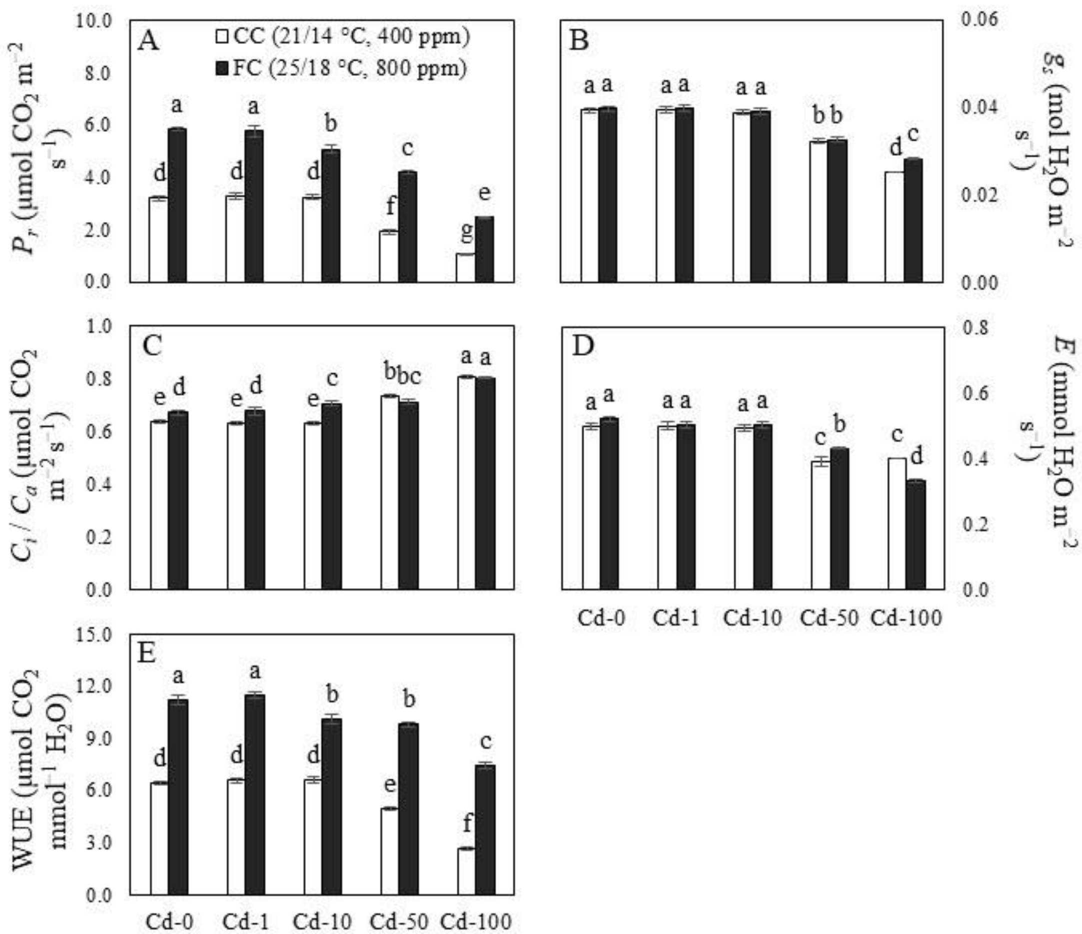

Fig. 5. Leaf gas exchange parameters of rapeseed (*Brassica napus*) exposed to Cd treatments (Cd-0, Cd-1, Cd-10, Cd-50, and Cd-100) under current climate (CC) and future climate (FC) conditions. [A] Photosynthetic rate (P_r); [B] Stomatal conductance (g_s); [C] The ratio of intercellular to ambient CO_2 concentration (C_i/C_a); [D] Transpiration rate (E); [E] Water use efficiency (WUE). Vertical bars represent ± SE of the mean ($n = 9$); Different letters indicate significant differences among the treatments according to Fischer's LSD ($p \leq 0.05$).

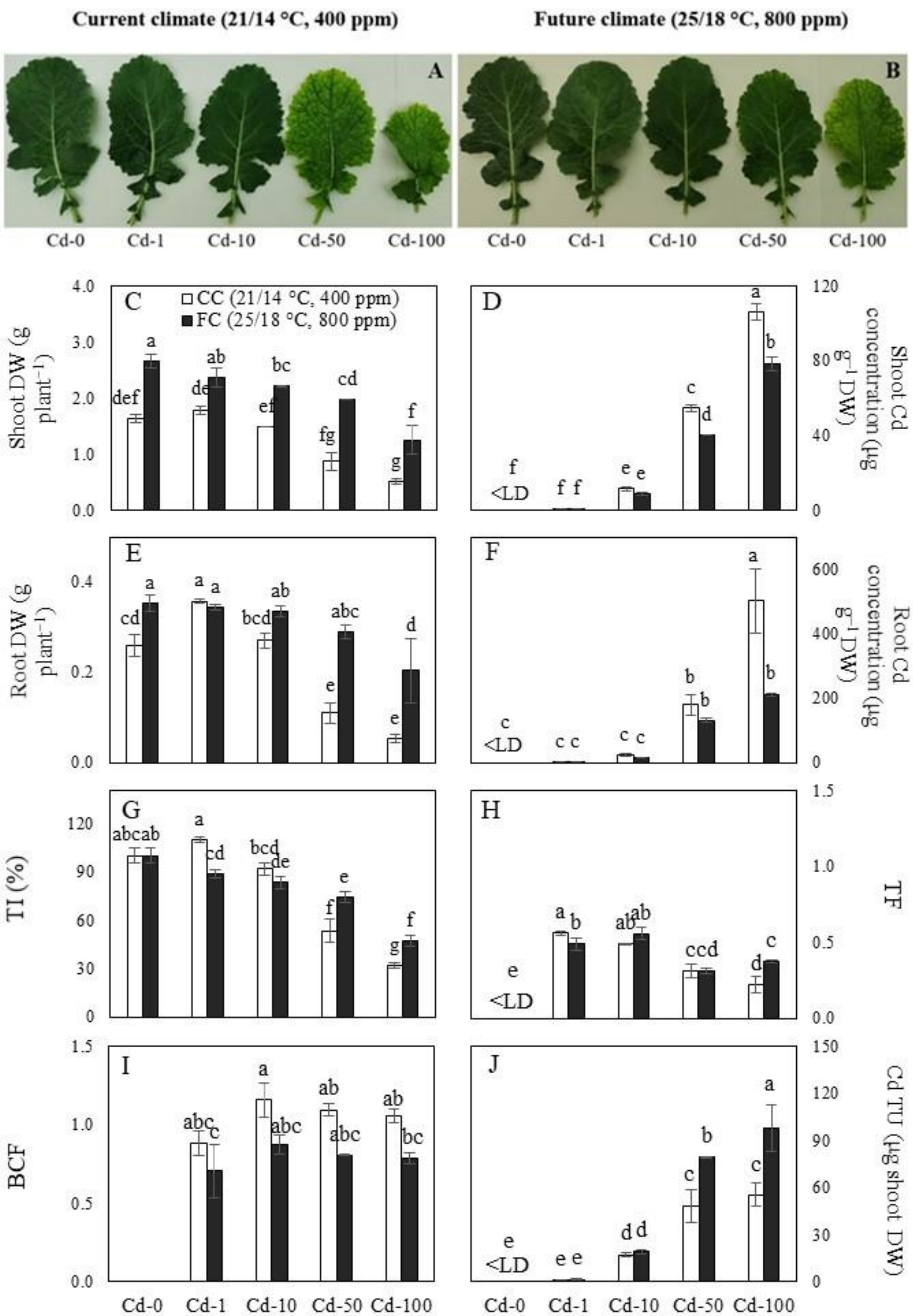

Fig. 6. A and B show visual symptoms on rapeseed (*Brassica napus*) leaves exposed to Cd treatments (Cd-0, Cd-1, Cd-10, Cd-50, and Cd-100) under current climate (CC) and future climate (FC) conditions,

respectively, at the end of the experiment. C-J shows shoot dry weight (DW), cadmium (Cd) concentration in shoots, root dry weight, Cd concentration in roots, Cd tolerance index (TI), translocation factor (TF), bioconcentration factor (BCF), and total Cd uptake (TU) index of rapeseed exposed to the same Cd treatments under CC and FC. Vertical bars represent ± SE of the mean (n = 3); < LD = below the detection limit.

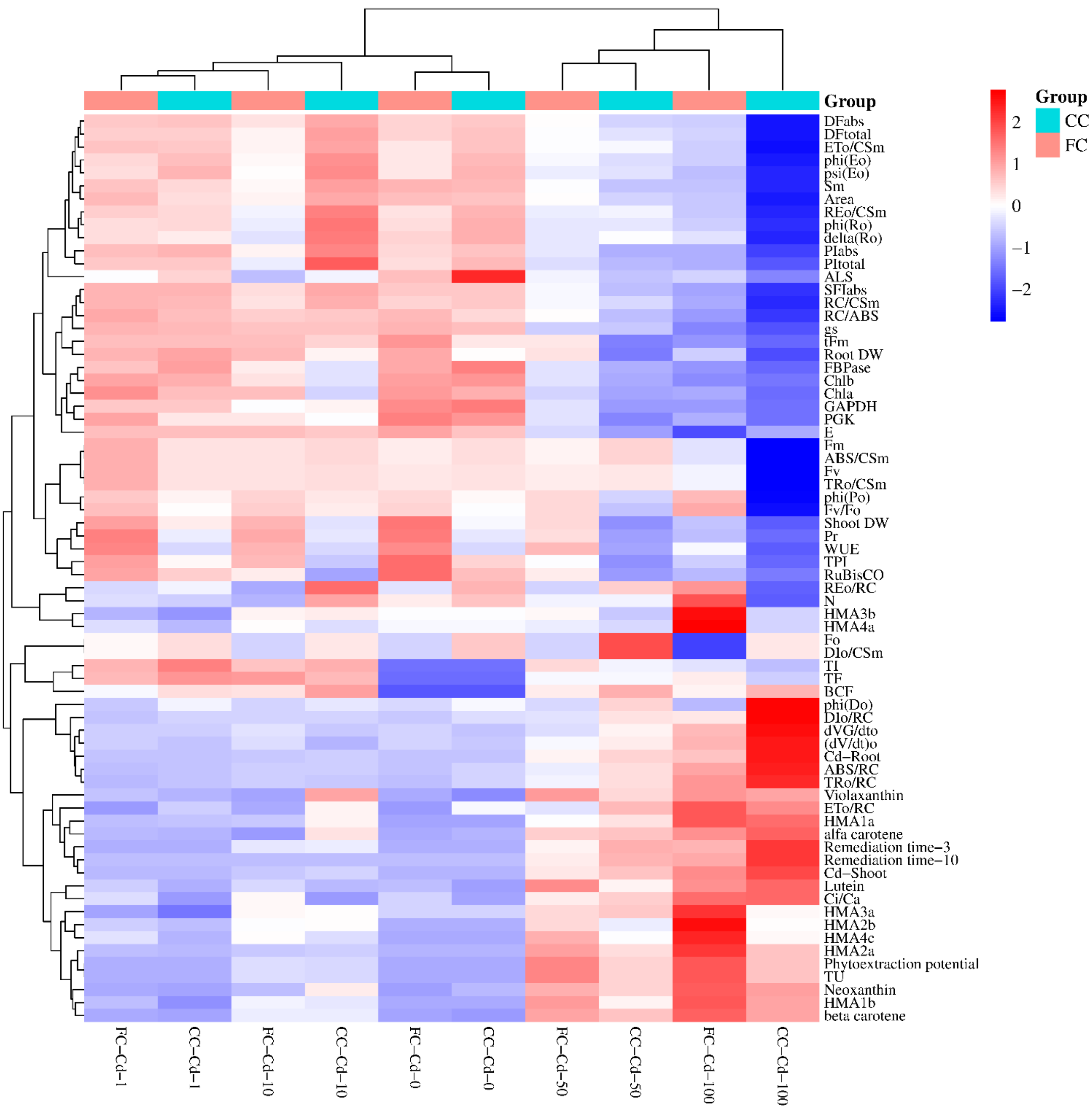

Fig. 7. Hierarchical Clustering Heatmap of growth, the physiological, biochemical, and molecular response, and phytoextraction efficiency of *Brassica napus* grown in Cd-contaminated soil (Cd-1−Cd-100) compared to control plants (Cd-0) under current climate (CC) and future climate (FC) conditions. A hierarchical clustering was performed using the Euclidean distance and the complete linkage method on both treatments (columns) and measured parameters (rows).

Supplemental materials

Table S1. Main physical and chemical characteristics of soil used in this study.

Soil properties	Means ± SE
pH 1 mol L^{-1} KCl	6.7 ± 0.1
N_{min} (mg kg^{-1})	22 ± 0.3
P_2O_5 (mg kg^{-1})	121 ± 4.5
K_2O (mg kg^{-1})	68 ± 1.0
Available S (mg kg^{-1})	2.7 ± 0.1
Available Ca (mg kg^{-1})	1588 ± 26.5
Available Mg (mg kg^{-1})	269 ± 4.5
C (%)	0.81 ± 0.01
Humus (%)	1.40 ± 0.02
SOM (%)	1.90 ± 0.01
EC (mS m^{-1})	6.6 ± 0.08

Table S2. The primer sequences of HMAs for qRT-PCR assay

Genes	Forward Primers	Reverse Primers
BnaHMA1a	TTCCCTCTCGTCGGAGTGTCA	GCAATCCTCCTTCAAGAGCGTT
BnaHMA1b	TCTCTCCTCTGTGAAACAAAGACTGA	TGAGAGCTGCGGGTTCCATAT
BnaHMA2a	GAAGGCATTTTTGGGAAGATTGAT	AACTCCGGCTAGTGTCTCTCCAAG
BnaHMA2b	CTCTCTGTCCCTCGGCTACCTC	ATGACGGTTCTTGACGGCAC
BnaHMA3a	GCAGTTGATGTAGACGAGGTTGGA	CATTTTCGCAACCACGCAGTC
BnaHMA3b	GAATAGAAGTTGATGTAGATGAGGTTG	CATTTTCGCAACCACGCAGTC
BnaHMA4a	TGGCCTTTTGAATCTCGATGTATC	CAAAAAACGAGAAATACTTGAGGCA
BnaHMA4c	GGAGAGATAACTATGGCATGTGAGG	CTTCCTTCAAACCACAAACAGACAT
BnaActin	CTGACCGTATGAGCAAAG	CCACCGAACCAGAAGGCAGA

Table S3. The abbreviations, formulas and definitions of JIP-test parameters, derived using data extracted from the fast fluorescence transient O-J-I-P, where O is for origin (the minimum fluorescence Fo), J and I for two intermediate levels at 2 ms and 30 ms (F_J and F_I), and P for peak (F_P, or Fm, when the fluorescence is maximal), used in this study. Here, PSI, PSII, RC, CS, Q_A, and PQ are for photosystem I, photosystem II, active PSII reaction centers, the cross section of PSII (i.e., the surface of the excited photosynthetic sample, which includes the photosynthetic response of both active and inactive RCs), the first plastoquinone electron acceptor of PSII, and plastoquinone, respectively.

Parameters	Formulas	Definitions	References*
Extracted and technical fluorescence parameters			
Fo		Minimum fluorescence intensity at 50 μs, when all PSII RCs are assumed to be open	1−3
Fm	$= F_P$	Maximum fluorescence intensity recorded under saturating illumination at the peak P of OJIP, when all PSII RCs are closed	1−4
Fv	= Fm – Fo	Maximum variable fluorescence	1−5
Fv/Fo	$= kp/k_N$ = (Fm – Fo)/Fo	The maximum ratio of quantum yields of photochemical and non-photochemical energy quenching in PSII RC, which is also related to maximal efficiency of the water-splitting or oxygen-evolving complex on the donor side of PSII, which is considered to be the most sensitive link in the photosynthetic chain of electron transport	1, 3, 6
dVG/dto		Expression of excitation energy transfer between RCs	1, 3
(dV/dt)o	$= Mo \approx 4(F_{0.3ms} - F_{0.05ms})/Fv$	Initial slope (in ms^{-1}) of the O-J fluorescence rise, which corresponds to the maximal rate of the accumulation of the fraction of closed RCs (expresses the rate of the RCs' closure)	1, 3, 5−7
tFm		Time to reach Fm, in ms	1, 2, 4, 7, 8
N		The turnover number that indicates how many times Q_A has been reduced in the time span from 0 to tFm (number of Q_A redox turnovers until Fm is reached)	1, 2, 7
Area		The total complementary area above the OJIP curve between Fo and Fm and the Fm	1−4, 6−8
Sm	= Area/Fv	Normalized area expresses the energy needed to close all RCs during the multiple turn-over in the Q_A reduction (closure of RCs) and is proportional to the pool size of the electron acceptors on the reducing side of PSII and therefore related to the number of electron carriers per electron transport chain	1−5, 7, 8
Quantum yields and efficiencies/probabilities			
φPo	= Fv/Fm = TRo/ABS = 1 − Fo/Fm	Maximum quantum yield of primary photochemistry reactions in PSII RC	1−8
ψEo	$= ETo/TRo = 1 - V_J$	Efficiency/probability that PSII trapped electron moves future than Q_A^- (i.e. is transferred from Q_A^- to PQ)	2−8
φEo	= ETo/ABS = φPo × ψEo	Quantum yield of electron transport (ET) from Q_A^- to PQ	2−7, 8
δRo	$= REo/ETo = (1 - V_I)/\psi Eo$	Efficiency/probability with which an electron from the intersystem electron carriers is transferred to reduce end electron acceptors at the PSI acceptor side	3−6, 8
φRo	$= REo/ABS = \varphi Po \times (1 - V_I)$	Quantum yield for reduction of end electron acceptors at the PSI acceptor side	3−5, 8
φDo	= Fo/Fm = 1 − φPo	Quantum yield of energy dissipation in PSII antenna	3, 5
Specific energy fluxes per active (Q_A reducing) PSII reaction centre (RC)			
ABS/RC	$= (Mo/V_J)/\varphi Po$	Absorption flux of antenna Chls per acive PSII RC (also a measure of PSII apparent antenna size)	1−8
TRo/RC	$= Mo/V_J$	Maximum trapped energy flux leading to Q_A reduction per active PSII RC	2−8
DIo/RC	= ABS/RC – TRo/RC	Dissipated energy flux per active PSII RC in processes other than trapping	1, 3, 5−7
ETo/RC	$= (Mo/V_J) \times \psi Eo$	Electron transport flux further than Q_A^- (i.e. from Q_A^- to PQ) per active PSII RC	1−8
REo/RC	$= (Mo/V_J) \times (1 - V_I)$	Electron flux leading to the reduction of the PSI end acceptor per active PSII RC	3−5, 8
RC/ABS	$= \varphi Po \times (V_J/Mo) = (ABS/RC)^{-1}$	Density of active RCs on PSII antenna Chl *a* basis (reciprocal of ABS/RC)	2, 8
Phenomenological energy fluxes per exited cross section (CSm, subscript m refers to time Fm) of PSII			
ABS/CSm	≈ Fm	Absorbed photon flux of antenna Chls per excited CSm of PSII	2, 5, 7
TRo/CSm	= φPo × ABS/CSm	Maximum trapped energy flux leading to Q_A reduction per excited CSm of PSII	2, 5, 7
DIo/CSm	= ABS/CSm – TRo/CSm	Dissipated energy flux per excited CSm of PSII in processes other than trapping	2, 7
ETo/CSm	= φEo × ABS/CSm	Electron transport flux further than Q_A^- (i.e. from Q_A^- to PQ) per excited CSm of PSII	2, 5, 7
REo/CSm	= φRo × ABS/CSm	Electron transport flux leading to the reduction of the PSI end acceptor per excited CSm of PSII	5
RC/CSm	$= \varphi Po \times (V_J/Mo) \times Fm$	Density of active RCs per excited CSm of PSII	2, 6, 7
Performance indexes on absorption basis (combination of parameters expressing partial potentials at steps of energy bifurcations of PSII and of specific electron transport reactions)			
PIabs	= (RC/ABS) × [φPo/(1 − φPo)] × [ψEo/(1 − ψEo)]	Performance index (potential) for energy conservation from photons absorbed by PSII antenna to the reduction of intersystem electron acceptors	1−8
PItotal	= PIabs × [δRo/(1 − δRo)]	Performance index for energy conservation from photons absorbed by PSII antenna to the reduction of PSI end acceptors	1, 3−5, 8
SFIabs	= RC/ABS × φPo × ψEo	Structure-function index, which reflects changes that "favor" photosynthesis	5
Driving forces on absorption basis			
DFabs	= log(PIabs)	The driving force for the photochemical activity of the processes evaluated by the PIabs	1, 5, 7
DFtotal	= log(PItotal)	The total driving force for the photochemical activity of the processes evaluated by the PItotal	5, 7

* – 1 (Samborska et al., 2019); 2 (Kumar et al., 2020); 3 (Esmaeilizadeh et al., 2021); 4 (Stirbet and Govindjee, 2011); 5 (Stirbet et al., 2018); 6 (Kalaji et al., 2018); 7 (Strasser et al., 2000); 8 (Strasser et al., 2010)

Table S4. The results (F values) of two-way ANOVA analysis for the effect of Cd treatment, climate, and interaction between these two factors on analyzed parameters. *, **, *** – significant effect at $p \leq 0.05$, $p \leq 0.01$, and $p \leq 0.001$, respectively.

Factors	***Growth parameters and Cd content***				***Phytoextraction efficiency***			
	Shoot DW	Root DW	Cd_{shoot}	Cd_{root}	BCF	TF	TI	TU
Cd	31.81***	28.46***	1306.33***	64.38***	1.78	152.21***	115.24***	108.04***
Climate	101.65***	39.05***	85.64***	17.47***	11.25**	2.71	0.5	24.00***
Cd × Climate	1.57	5.31**	29.02***	10.50***	0.15	5.11**	16.40***	8.25**

Factors	***Phytoextraction potential***	***Hypotetical remediation time***		***Gas exchange parameters***				
		to pollution limit	to lower SGV (e)	P_r	g_s	C_i/C_a	E	WUE
Cd	77.99***	23.88**	14.37*	253.17***	170.35***	117.84***	96.19***	161.98***
Climate	20.26**	11.92*	11.27*	1005.41***	4.69*	25.03***	0.04	1583.21***
Cd × Climate	6.48*	3.01	1.14	10.95***	2.08	10.63***	9.35***	5.23**

Factors	***JIP-test parameters***							
	Fo	Fm	Fv	Fv/Fo	dVG/dto	(dV/dt)o	tFm	N
Cd	1.52	7.96***	8.03***	3.40*	11.20***	11.64***	20.68***	0.18
Climate	9.90**	2.87	5.36*	24.73***	2.08	1.02	12.04**	0.24
Cd × Climate	1.00	3.38*	4.06*	6.07**	2.29	2.13	2.32	1.81

Factors	***JIP-test parameters***							
	Area	Sm	φPo	ψEo	φEo	δRo	φRo	φDo
Cd	22.34***	20.98***	3.5*	12.41***	11.82***	10.14***	19.35***	3.53*
Climate	5.29*	3.36	16.6***	0.16	0.09	0.03	0.35	16.60***
Cd × Climate	6.12**	5.57**	5.2**	4.44**	4.90**	7.10***	10.20***	5.22**

Factors	***JIP-test parameters***							
	ABS/RC	TRo/RC	DIo/RC	ETo/RC	REo/RC	RC/ABS	ABS/CSm	TRo/CSm
Cd	11.43***	12.21***	7.79***	4.85**	0.29	15.03***	7.96***	8.03***
Climate	3.06	2.08	6.15*	2.64	0.76	3.96	2.87	5.36*
Cd × Climate	1.07	0.66	2.61	0.69	3.57*	0.73	3.38*	4.06*

Factors	***JIP-test parameters***							
	DIo/CSm	ETo/CSm	REo/CSm	RC/CSm	PIabs	PItotal	SFIabs	DFabs
Cd	1.52	12.00***	0.29	15.03***	17.00***	24.54***	17.36***	12.91***
Climate	9.90**	0.63	0.76	1.01	0.12	1.55	1.39	2.15
Cd × Climate	1.00	4.48**	3.57*	2.00	3.56*	8.27***	1.99	3.77*

Factors	***JIP-test parameters***	***Photosynthesis-related enzymes***						***Photosynthetic pigments***
	DFtotal	Rubisco	FBPase	TPI	PGK	GAPDH	ALS	Chl *a*
Cd	24.54***	90.18***	35.51***	17.69***	27.48***	8.24***	14.98***	31.43***
Climate	1.55	103.66***	0.96	38.51***	11.43**	0.28	1.62	15.64***
Cd × Climate	8.27***	3.73*	2.17	0.13	0.75	0.35	4.12*	0.95

Factors	***Photosynthetic pigments***	***Antioxidant pigments***					***HMA genes expression***	
	Chl *b*	α-carotene	β-carotene	Neoxanthin	Violaxanthin	Lutein	*BNAHMA1a*	*BNAHMA1b*
Cd	83.57***	30.83***	53.71***	25.40***	17.21***	13.14***	28.94***	13.94***
Climate	7.59*	5.94*	3.07	0.02	0.43	1.78	0.94	4.00
Cd × Climate	1.92	2.77	1.06	2.42	5.60**	1.02	0.85	0.63

Factors	***HMA genes expression***					
	BNAHMA2a	*BNAHMA2b*	*BNAHMA3a*	*BNAHMA3b*	*BNAHMA4a*	*BNAHMA4c*
Cd	55.50***	9.48***	3.24*	4.61**	24.62***	43.02***
Climate	14.35**	7.22*	1.21	6.88*	51.41***	47.67***
Cd × Climate	6.45**	3.98*	0.86	3.58*	25.05***	11.17***

Table S5. Values expressed as mean ± SE (n = 3) of JIP-test parameters of rapeseed (*Brassica napus*) exposed to Cd treatments (Cd-0, Cd-1, Cd-10, Cd-50, and Cd-100) under current climate (CC, 21/14 °C, 400 ppm) and future climate (FC, 25/18 °C, 800 ppm) conditions. Different letters following values in the same row indicate a significant difference between treatments (Fischer's LSD, $p \leq 0.05$).

Parameter	Cd-0		Cd-1		Cd-10		Cd-50		Cd-100	
	CC	FC	CC	FC	CC	FC	CC	FC	CC	FC
Fo	468 ± 6.9^{ab}	446 ± 11.5^{bc}	464 ± 3.5^{ab}	458 ± 12.8^{ab}	461 ± 5.5^{ab}	445 ± 6.8^{bc}	498 ± 27.1^{a}	445 ± 12.7^{bc}	461 ± 19.9^{ab}	412 ± 21.3^{c}
Fm	3063 ± 32.7^{a}	3023 ± 25.5^{a}	3051 ± 76.4^{a}	3163 ± 79.2^{a}	3067 ± 51.8^{a}	3040 ± 57.5^{a}	3077 ± 60.0^{a}	3014 ± 105.9^{a}	2372 ± 179.8^{b}	2904 ± 158.4^{a}
Fv	2594 ± 33.3^{a}	2578 ± 21.8^{a}	2587 ± 74.1^{a}	2705 ± 67.2^{a}	2607 ± 49.4^{a}	2594 ± 57.7^{a}	2579 ± 40.3^{a}	2569 ± 93.2^{a}	1911 ± 185.8^{b}	2492 ± 138.9^{a}
Fv/Fo	5.54 ± 0.12^{ab}	5.79 ± 0.15^{ab}	5.57 ± 0.14^{ab}	5.91 ± 0.06^{a}	5.66 ± 0.10^{ab}	5.83 ± 0.16^{a}	5.21 ± 0.26^{b}	5.77 ± 0.05^{ab}	4.17 ± 0.48^{c}	6.06 ± 0.14^{a}
dVG/dto	0.12 ± 0.022^{c}	0.13 ± 0.002^{c}	0.12 ± 0.005^{c}	0.13 ± 0.011^{c}	0.12 ± 0.005^{c}	0.14 ± 0.011^{b}	0.18 ± 0.005^{b}	0.14 ± 0.013^{b}	0.38 ± 0.090^{a}	0.23 ± 0.037^{b}
(dV/dt)o	0.30 ± 0.016^{c}	0.32 ± 0.013^{c}	0.29 ± 0.020^{c}	0.31 ± 0.025^{c}	0.27 ± 0.006^{c}	0.34 ± 0.018^{b}	0.44 ± 0.010^{b}	0.39 ± 0.035^{b}	0.81 ± 0.178^{a}	0.54 ± 0.093^{b}
tFm	600 ± 0.0^{b}	733 ± 33.3^{a}	667 ± 33.3^{ab}	667 ± 33.3^{ab}	633 ± 33.3^{ab}	667 ± 33.3^{ab}	367 ± 33.3^{c}	600 ± 0.0^{b}	327 ± 36.7^{c}	397 ± 101.7^{c}
N	297524 ± 8537^{ab}	288007 ± 3903^{ab}	271132 ± 4368^{ab}	275158 ± 4552^{ab}	305968 ± 10676^{ab}	265457 ± 7322^{ab}	280372 ± 19800^{ab}	280651 ± 7711^{ab}	243025 ± 21818^{b}	326066 ± 67533^{a}
Area	83289 ± 2517^{ab}	83593 ± 1263^{ab}	78774 ± 2757^{ab}	85223 ± 3158^{ab}	87496 ± 3050^{a}	74855 ± 1972^{abc}	64937 ± 3170^{c}	72866 ± 6994^{bc}	32442 ± 7549^{d}	63183 ± 6963^{c}
Sm	32.1 ± 1.0^{ab}	32.4 ± 0.6^{ab}	30.4 ± 0.5^{ab}	31.6 ± 1.6^{ab}	33.6 ± 1.1^{a}	28.8 ± 0.1^{bc}	25.2 ± 1.5^{c}	28.2 ± 1.7^{bc}	16.6 ± 2.5^{d}	25.3 ± 2.0^{c}
φPo	0.85 ± 0.003^{ab}	0.85 ± 0.003^{ab}	0.85 ± 0.003^{ab}	0.86 ± 0.001^{ab}	0.85 ± 0.002^{ab}	0.85 ± 0.004^{ab}	0.84 ± 0.007^{b}	0.85 ± 0.001^{ab}	0.80 ± 0.018^{c}	0.86 ± 0.003^{a}
ψEo	0.67 ± 0.009^{ab}	0.64 ± 0.008^{abcd}	0.67 ± 0.014^{abc}	0.65 ± 0.006^{abcd}	0.70 ± 0.002^{a}	0.63 ± 0.011^{bcd}	0.61 ± 0.014^{cd}	0.61 ± 0.021^{bcd}	0.48 ± 0.060^{e}	0.58 ± 0.021^{d}
φEo	0.57 ± 0.008^{ab}	0.54 ± 0.009^{abc}	0.57 ± 0.012^{ab}	0.55 ± 0.006^{abc}	0.60 ± 0.001^{a}	0.53 ± 0.011^{abc}	0.51 ± 0.012^{bc}	0.52 ± 0.018^{bc}	0.39 ± 0.057^{d}	0.50 ± 0.019^{c}
δRo	0.41 ± 0.003^{ab}	0.39 ± 0.007^{abc}	0.38 ± 0.014^{bc}	0.38 ± 0.013^{abc}	0.44 ± 0.003^{a}	0.35 ± 0.002^{c}	0.36 ± 0.015^{bc}	0.35 ± 0.014^{c}	0.25 ± 0.032^{d}	0.35 ± 0.034^{c}
φRo	0.23 ± 0.004^{ab}	0.21 ± 0.004^{bc}	0.22 ± 0.012^{bc}	0.21 ± 0.009^{bc}	0.26 ± 0.002^{a}	0.19 ± 0.005^{cd}	0.19 ± 0.012^{cd}	0.19 ± 0.014^{cd}	0.10 ± 0.023^{e}	0.17 ± 0.016^{d}
φDo	1.15 ± 0.003^{bc}	1.15 ± 0.003^{bc}	1.15 ± 0.003^{bc}	1.14 ± 0.001^{bc}	1.15 ± 0.002^{bc}	1.15 ± 0.004^{bc}	1.16 ± 0.007^{b}	0.15 ± 0.001^{bc}	1.20 ± 0.018^{a}	1.14 ± 0.003^{c}
ABS/RC	1.10 ± 0.04^{c}	1.04 ± 0.02^{c}	1.05 ± 0.03^{c}	1.03 ± 0.07^{c}	1.07 ± 0.03^{c}	1.08 ± 0.04^{c}	1.33 ± 0.02^{bc}	1.17 ± 0.04^{bc}	1.90 ± 0.26^{a}	1.49 ± 0.23^{b}
TRo/RC	0.93 ± 0.03^{c}	0.89 ± 0.02^{c}	0.89 ± 0.02^{c}	0.88 ± 0.06^{c}	0.91 ± 0.02^{c}	0.92 ± 0.03^{c}	1.11 ± 0.02^{bc}	1.00 ± 0.04^{c}	1.51 ± 0.18^{a}	1.28 ± 0.19^{ba}
DIo/RC	0.17 ± 0.01^{b}	0.15 ± 0.01^{b}	0.16 ± 0.01^{b}	0.15 ± 0.01^{b}	0.16 ± 0.01^{b}	0.16 ± 0.01^{b}	0.21 ± 0.01^{b}	0.17 ± 0.01^{b}	0.38 ± 0.09^{a}	0.21 ± 0.04^{b}
ETo/RC	0.63 ± 0.02^{bcd}	0.57 ± 0.00^{d}	0.60 ± 0.01^{bcd}	0.57 ± 0.03^{d}	0.64 ± 0.02^{abcd}	0.58 ± 0.01^{cd}	0.68 ± 0.03^{abc}	0.61 ± 0.00^{bcd}	0.71 ± 0.00^{ab}	0.74 ± 0.10^{a}
REo/RC	0.26 ± 0.01^{ab}	0.22 ± 0.01^{abc}	0.23 ± 0.01^{abc}	0.22 ± 0.00^{abc}	0.28 ± 0.00^{a}	0.20 ± 0.00^{b}	0.25 ± 0.02^{ab}	0.22 ± 0.01^{abc}	0.18 ± 0.02^{c}	0.27 ± 0.06^{ab}
RC/ABS	0.92 ± 0.04^{a}	0.96 ± 0.02^{a}	0.95 ± 0.03^{a}	0.98 ± 0.06^{a}	0.93 ± 0.03^{a}	0.93 ± 0.03^{a}	0.76 ± 0.01^{bc}	0.86 ± 0.03^{ab}	0.55 ± 0.08^{d}	0.70 ± 0.10^{c}
ABS/CSm	3063 ± 32.7^{a}	3023 ± 25.5^{a}	3051 ± 76.4^{a}	3163 ± 79.2^{a}	3067 ± 51.8^{a}	3040 ± 57.5^{a}	3077 ± 60.0^{a}	3014 ± 105.9^{a}	2372 ± 179.8^{b}	2904 ± 158.4^{a}
TRo/CSm	2594 ± 33.3^{a}	2578 ± 21.8^{a}	2587 ± 74.1^{a}	2705 ± 67.2^{a}	2607 ± 49.4^{a}	2594 ± 57.7^{a}	2579 ± 40.3^{a}	2569 ± 93.2^{a}	1911 ± 185.8^{b}	2492 ± 138.9^{a}
DIo/CSm	468 ± 6.9^{ab}	446 ± 11.5^{bc}	464 ± 3.5^{ab}	458 ± 12.8^{ab}	461 ± 5.5^{ab}	445 ± 6.8^{bc}	498 ± 27.1^{a}	445 ± 12.7^{bc}	461 ± 19.9^{ab}	412 ± 21.3^{c}
ETo/CSm	1750 ± 19.0^{a}	1647 ± 24.5^{ab}	1744 ± 73.4^{a}	1752 ± 37.9^{a}	1832 ± 33.2^{a}	1626 ± 61.6^{ab}	1566 ± 15.1^{ab}	1582 ± 106.0^{ab}	939 ± 211.8^{c}	1459 ± 134.9^{b}
REo/CSm	713 ± 7.0^{ab}	640 ± 6.4^{bc}	658 ± 43.2^{bc}	673 ± 24.4^{bc}	799 ± 14.7^{a}	570 ± 24.4^{cd}	572 ± 29.6^{cd}	561 ± 58.7^{cd}	243 ± 71.0^{e}	508 ± 52.5^{d}
RC/CSm	2234 ± 98.4^{ab}	2176 ± 60.9^{ab}	2316 ± 155.7^{a}	2351 ± 138.2^{a}	2369 ± 93.2^{a}	2078 ± 133.7^{ab}	1684 ± 47.9^{bc}	1872 ± 184.8^{abc}	670 ± 393.3^{d}	1415 ± 320.5^{c}
PIabs	10.6 ± 0.8^{abc}	9.9 ± 0.8^{abc}	11.1 ± 1.2^{ab}	10.7 ± 1.0^{abc}	12.5 ± 0.5^{a}	9.2 ± 0.9^{bc}	6.1 ± 0.3^{d}	8.0 ± 1.0^{cd}	2.6 ± 1.3^{e}	6.2 ± 1.5^{d}
PItotal	7.3 ± 0.5^{b}	6.3 ± 0.4^{bcd}	6.8 ± 1.0^{bc}	6.8 ± 1.0^{bc}	9.7 ± 0.4^{a}	4.9 ± 0.5^{cde}	3.5 ± 0.4^{e}	4.4 ± 0.8^{de}	1.0 ± 0.5^{f}	3.2 ± 0.5^{e}
SFIabs	0.52 ± 0.025^{a}	0.52 ± 0.020^{a}	0.55 ± 0.028^{a}	0.55 ± 0.041^{a}	0.56 ± 0.016^{a}	0.50 ± 0.026^{a}	0.38 ± 0.002^{b}	0.45 ± 0.031^{ab}	0.22 ± 0.065^{c}	0.35 ± 0.064^{b}
DFabs	1.02 ± 0.035^{ab}	0.99 ± 0.036^{abc}	1.04 ± 0.044^{a}	1.03 ± 0.043^{ab}	1.10 ± 0.017^{a}	0.96 ± 0.043^{abc}	0.78 ± 0.024^{bc}	0.90 ± 0.056^{abc}	0.31 ± 0.217^{d}	0.76 ± 0.102^{c}
DFtotal	0.86 ± 0.034^{ab}	0.80 ± 0.031^{abc}	0.82 ± 0.064^{abc}	0.82 ± 0.068^{abc}	0.98 ± 0.020^{a}	0.69 ± 0.046^{abcd}	0.54 ± 0.046^{cd}	0.63 ± 0.083^{bcd}	−0.17 ± 0.277^{e}	0.49 ± 0.061^{d}

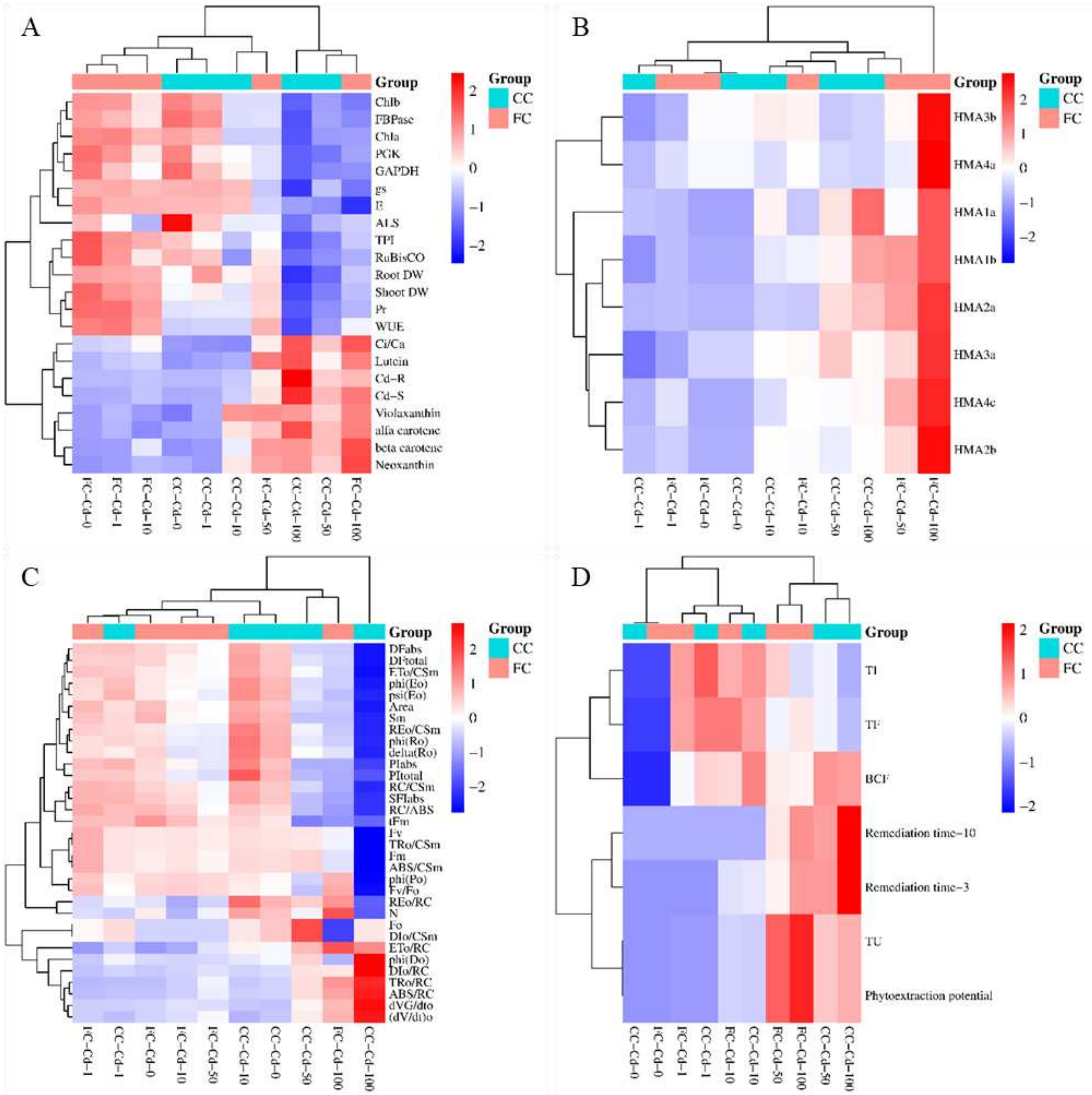

Fig. S1. Hierarchical Clustering Heatmap displaying (A) shoot and root dry weight (DW), Cd content in shoots (Cd-S) and roots (Cd-R), leaf gas exchange, Calvin cycle-related enzymes activity, and photosynthetic and antioxidant pigments content (B) relative expression levels of heavy metal ATPases (HMAs) genes (C) JIP-test parameters and (D) phytoextraction efficiency-related parameters and hypothetical remediation time to pollution limit of 3 mg kg^{-1} (remediation time-3) and lower soil guideline value of 10 mg kg^{-1} based on the ecological risk (remediation time-10) of *Brassica napus* grown in Cd-contaminated soil (Cd-1−Cd-100) compared to control plants (Cd-0) under current climate (CC) and future climate (FC) conditions. A hierarchical clustering was performed using the Euclidean distance and the complete linkage method on both treatments (columns) and measured parameters (rows).